

An Improved Measurement of R_b using a Double Tagging Method

The OPAL Collaboration

Abstract

This paper describes an update of the double tagging measurement of the fraction, R_b , of $Z^0 \rightarrow b\bar{b}$ events in hadronic Z^0 decays, with statistics improved by including the data collected in 1994. The presence of electrons or muons from semileptonic decays of bottom hadrons and the detection of bottom hadron decay vertices were used together to obtain an event sample enriched in $Z^0 \rightarrow b\bar{b}$ decays. The efficiency of the $b\bar{b}$ event tagging was obtained from the data by comparing the numbers of events having a bottom signature in either one or both thrust hemispheres. Efficiency correlations between opposite event hemispheres are small ($< 0.5\%$) and well understood through comparisons between the real and simulated data samples. A value of

$$R_b = 0.2175 \pm 0.0014 \pm 0.0017$$

was obtained, where the first error is statistical and the second systematic. The uncertainty on the decay width $\Gamma(Z^0 \rightarrow c\bar{c})$ is not included in these errors. The result depends on R_c as follows:

$$\frac{\Delta R_b}{R_b} = -0.084 \frac{\Delta R_c}{R_c},$$

where ΔR_c is the deviation of R_c from the value 0.172 predicted by the Standard Model.

(Submitted to Zeitschrift für Physik C)

The OPAL Collaboration

K. Ackerstaff⁸, G. Alexander²³, J. Allison¹⁶, N. Altekamp⁵, K. Ametewee²⁵, K.J. Anderson⁹,
 S. Anderson¹², S. Arcelli², S. Asai²⁴, D. Axen²⁹, G. Azuelos^{18,a}, A.H. Ball¹⁷, E. Barberio⁸,
 R.J. Barlow¹⁶, R. Bartoldus³, J.R. Batley⁵, J. Bechtluft¹⁴, C. Beeston¹⁶, T. Behnke⁸, A.N. Bell¹,
 K.W. Bell²⁰, G. Bella²³, S. Bentvelsen⁸, P. Berlich¹⁰, S. Bethke¹⁴, O. Biebel¹⁴, A. Biguzzi², V. Blobel²⁷,
 I.J. Bloodworth¹, J.E. Bloomer¹, M. Bobinski¹⁰, P. Bock¹¹, H.M. Bosch¹¹, M. Boutemour³⁴,
 B.T. Bouwens¹², S. Braibant¹², R.M. Brown²⁰, H.J. Burckhart⁸, C. Burgard⁸, R. Bürgin¹⁰,
 P. Capiluppi², R.K. Carnegie⁶, A.A. Carter¹³, J.R. Carter⁵, C.Y. Chang¹⁷, D.G. Charlton^{1,b},
 D. Chrisman⁴, P.E.L. Clarke¹⁵, I. Cohen²³, J.E. Conboy¹⁵, O.C. Cooke¹⁶, M. Cuffiani², S. Dado²²,
 C. Dallapiccola¹⁷, G.M. Dallavalle², S. De Jong¹², L.A. del Pozo⁸, K. Desch³, M.S. Dixit⁷, E. do Couto
 e Silva¹², M. Doucet¹⁸, E. Duchovni²⁶, G. Duckeck³⁴, I.P. Duerdoth¹⁶, J.E.G. Edwards¹⁶,
 P.G. Estabrooks⁶, H.G. Evans⁹, M. Evans¹³, F. Fabbri², P. Fath¹¹, F. Fiedler²⁷, M. Fierro²,
 H.M. Fischer³, R. Folman²⁶, D.G. Fong¹⁷, M. Foucher¹⁷, A. Fürtjes⁸, P. Gagnon⁷, A. Gaidot²¹,
 J.W. Gary⁴, J. Gascon¹⁸, S.M. Gascon-Shotkin¹⁷, N.I. Geddes²⁰, C. Geich-Gimbel³, F.X. Gentit²¹,
 T. Geralis²⁰, G. Giacomelli², P. Giacomelli⁴, R. Giacomelli², V. Gibson⁵, W.R. Gibson¹³,
 D.M. Gingrich^{30,a}, D. Glenzinski⁹, J. Goldberg²², M.J. Goodrick⁵, W. Gorn⁴, C. Grandi², E. Gross²⁶,
 J. Grunhaus²³, M. Gruwé⁸, C. Hajdu³², G.G. Hanson¹², M. Hansroul⁸, M. Hapke¹³, C.K. Hargrove⁷,
 P.A. Hart⁹, C. Hartmann³, M. Hauschild⁸, C.M. Hawkes⁵, R. Hawkings⁸, R.J. Hemingway⁶,
 M. Herndon¹⁷, G. Herten¹⁰, R.D. Heuer⁸, M.D. Hildreth⁸, J.C. Hill⁵, S.J. Hillier¹, T. Hilse¹⁰,
 P.R. Hobson²⁵, R.J. Homer¹, A.K. Honma^{28,a}, D. Horváth^{32,c}, R. Howard²⁹, R.E. Hughes-Jones¹⁶,
 D.E. Hutchcroft⁵, P. Igo-Kemenes¹¹, D.C. Imrie²⁵, M.R. Ingram¹⁶, K. Ishii²⁴, A. Jawahery¹⁷,
 P.W. Jeffreys²⁰, H. Jeremie¹⁸, M. Jimack¹, A. Joly¹⁸, C.R. Jones⁵, G. Jones¹⁶, M. Jones⁶,
 R.W.L. Jones⁸, U. Jost¹¹, P. Jovanovic¹, T.R. Junk⁸, D. Karlen⁶, K. Kawagoe²⁴, T. Kawamoto²⁴,
 R.K. Keeler²⁸, R.G. Kellogg¹⁷, B.W. Kennedy²⁰, B.J. King⁸, J. Kirk²⁹, S. Kluth⁸, T. Kobayashi²⁴,
 M. Kobel¹⁰, D.S. Koetke⁶, T.P. Kokott³, M. Kolrep¹⁰, S. Komamiya²⁴, T. Kress¹¹, P. Krieger⁶, J. von
 Krogh¹¹, P. Kyberd¹³, G.D. Lafferty¹⁶, H. Lafoux²¹, R. Lahmann¹⁷, W.P. Lai¹⁹, D. Lanske¹⁴,
 J. Lauber¹⁵, S.R. Lautenschlager³¹, J.G. Layter⁴, D. Lazic²², A.M. Lee³¹, E. Lefebvre¹⁸, D. Lellouch²⁶,
 J. Letts², L. Levinson²⁶, C. Lewis¹⁵, S.L. Lloyd¹³, F.K. Loebinger¹⁶, G.D. Long¹⁷, M.J. Losty⁷,
 J. Ludwig¹⁰, A. Malik²¹, M. Mannelli⁸, S. Marcellini², C. Markus³, A.J. Martin¹³, J.P. Martin¹⁸,
 G. Martinez¹⁷, T. Mashimo²⁴, W. Matthews²⁵, P. Mättig³, W.J. McDonald³⁰, J. McKenna²⁹,
 E.A. Mckigney¹⁵, T.J. McMahon¹, A.I. McNab¹³, R.A. McPherson⁸, F. Meijers⁸, S. Menke³,
 F.S. Merritt⁹, H. Mes⁷, J. Meyer²⁷, A. Michelini², G. Mikenberg²⁶, D.J. Miller¹⁵, R. Mir²⁶, W. Mohr¹⁰,
 A. Montanari², T. Mori²⁴, M. Morii²⁴, U. Müller³, K. Nagai²⁶, I. Nakamura²⁴, H.A. Neal⁸, B. Nellen³,
 B. Nijhar¹⁶, R. Nisius⁸, S.W. O’Neale¹, F.G. Oakham⁷, F. Odorici², H.O. Ogren¹², N.J. Oldershaw¹⁶,
 T. Omori²⁴, M.J. Oreglia⁹, S. Orito²⁴, J. Pálincás^{33,d}, G. Pásztor³², J.R. Pater¹⁶, G.N. Patrick²⁰,
 J. Patt¹⁰, M.J. Pearce¹, S. Petzold²⁷, P. Pfeifenschneider¹⁴, J.E. Pilcher⁹, J. Pinfold³⁰, D.E. Plane⁸,
 P. Poffenberger²⁸, B. Poli², A. Posthaus³, H. Przysiezniak³⁰, D.L. Rees¹, D. Rigby¹, S. Robertson²⁸,
 S.A. Robins¹³, N. Rodning³⁰, J.M. Roney²⁸, A. Rooke¹⁵, E. Ros⁸, A.M. Rossi², M. Rosvick²⁸,
 P. Routenburg³⁰, Y. Rozen²², K. Runge¹⁰, O. Runolfsson⁸, U. Ruppel¹⁴, D.R. Rust¹², R. Rylko²⁵,
 K. Sachs¹⁰, E.K.G. Sarkisyan²³, M. Sasaki²⁴, C. Sbarra², A.D. Schaile³⁴, O. Schaille³⁴, F. Scharf³,
 P. Scharff-Hansen⁸, P. Schenk²⁷, B. Schmitt⁸, S. Schmitt¹¹, M. Schröder⁸, H.C. Schultz-Coulon¹⁰,
 M. Schulz⁸, M. Schumacher³, P. Schütz³, W.G. Scott²⁰, T.G. Shears¹⁶, B.C. Shen⁴,
 C.H. Shepherd-Themistocleous⁸, P. Sherwood¹⁵, G.P. Sirolì², A. Sittler²⁷, A. Skillman¹⁵, A. Skuja¹⁷,
 A.M. Smith⁸, T.J. Smith²⁸, G.A. Snow¹⁷, R. Sobie²⁸, S. Söldner-Rembold¹⁰, R.W. Springer³⁰,
 M. Sproston²⁰, A. Stahl³, M. Steiert¹¹, K. Stephens¹⁶, J. Steuerer²⁷, B. Stockhausen³, D. Strom¹⁹,
 F. Strumia⁸, P. Szymanski²⁰, R. Tafirout¹⁸, S.D. Talbot¹, S. Tanaka²⁴, P. Taras¹⁸, S. Tarem²²,
 M. Thiergen¹⁰, M.A. Thomson⁸, E. von Törne³, S. Towers⁶, I. Trigger¹⁸, T. Tsukamoto²⁴, E. Tsur²³,
 A.S. Turcot⁹, M.F. Turner-Watson⁸, P. Utzat¹¹, R. Van Kooten¹², G. Vasseur²¹, M. Verzocchi¹⁰,

P. Vikas¹⁸, M. Vincter²⁸, E.H. Vokurka¹⁶, F. Wäckerle¹⁰, A. Wagner²⁷, C.P. Ward⁵, D.R. Ward⁵, J.J. Ward¹⁵, P.M. Watkins¹, A.T. Watson¹, N.K. Watson⁷, P.S. Wells⁸, N. Vermes³, J.S. White²⁸, B.. Wilkens¹⁰, G.W. Wilson²⁷, J.A. Wilson¹, G. Wolf²⁶, S. Wotton⁵, T.R. Wyatt¹⁶, S. Yamashita²⁴, G. Yekutieli²⁶, V. Zacek¹⁸

¹School of Physics and Space Research, University of Birmingham, Birmingham B15 2TT, UK

²Dipartimento di Fisica dell' Università di Bologna and INFN, I-40126 Bologna, Italy

³Physikalisches Institut, Universität Bonn, D-53115 Bonn, Germany

⁴Department of Physics, University of California, Riverside CA 92521, USA

⁵Cavendish Laboratory, Cambridge CB3 0HE, UK

⁶Ottawa-Carleton Institute for Physics, Department of Physics, Carleton University, Ottawa, Ontario K1S 5B6, Canada

⁷Centre for Research in Particle Physics, Carleton University, Ottawa, Ontario K1S 5B6, Canada

⁸CERN, European Organisation for Particle Physics, CH-1211 Geneva 23, Switzerland

⁹Enrico Fermi Institute and Department of Physics, University of Chicago, Chicago IL 60637, USA

¹⁰Fakultät für Physik, Albert Ludwigs Universität, D-79104 Freiburg, Germany

¹¹Physikalisches Institut, Universität Heidelberg, D-69120 Heidelberg, Germany

¹²Indiana University, Department of Physics, Swain Hall West 117, Bloomington IN 47405, USA

¹³Queen Mary and Westfield College, University of London, London E1 4NS, UK

¹⁴Technische Hochschule Aachen, III Physikalisches Institut, Sommerfeldstrasse 26-28, D-52056 Aachen, Germany

¹⁵University College London, London WC1E 6BT, UK

¹⁶Department of Physics, Schuster Laboratory, The University, Manchester M13 9PL, UK

¹⁷Department of Physics, University of Maryland, College Park, MD 20742, USA

¹⁸Laboratoire de Physique Nucléaire, Université de Montréal, Montréal, Quebec H3C 3J7, Canada

¹⁹University of Oregon, Department of Physics, Eugene OR 97403, USA

²⁰Rutherford Appleton Laboratory, Chilton, Didcot, Oxfordshire OX11 0QX, UK

²¹CEA, DAPNIA/SPP, CE-Saclay, F-91191 Gif-sur-Yvette, France

²²Department of Physics, Technion-Israel Institute of Technology, Haifa 32000, Israel

²³Department of Physics and Astronomy, Tel Aviv University, Tel Aviv 69978, Israel

²⁴International Centre for Elementary Particle Physics and Department of Physics, University of Tokyo, Tokyo 113, and Kobe University, Kobe 657, Japan

²⁵Brunel University, Uxbridge, Middlesex UB8 3PH, UK

²⁶Particle Physics Department, Weizmann Institute of Science, Rehovot 76100, Israel

²⁷Universität Hamburg/DESY, II Institut für Experimental Physik, Notkestrasse 85, D-22607 Hamburg, Germany

²⁸University of Victoria, Department of Physics, P O Box 3055, Victoria BC V8W 3P6, Canada

²⁹University of British Columbia, Department of Physics, Vancouver BC V6T 1Z1, Canada

³⁰University of Alberta, Department of Physics, Edmonton AB T6G 2J1, Canada

³¹Duke University, Dept of Physics, Durham, NC 27708-0305, USA

³²Research Institute for Particle and Nuclear Physics, H-1525 Budapest, P O Box 49, Hungary

³³Institute of Nuclear Research, H-4001 Debrecen, P O Box 51, Hungary

³⁴Ludwigs-Maximilians-Universität München, Sektion Physik, Am Coulombwall 1, D-85748 Garching, Germany

^a and at TRIUMF, Vancouver, Canada V6T 2A3

^b and Royal Society University Research Fellow

^c and Institute of Nuclear Research, Debrecen, Hungary

^d and Department of Experimental Physics, Lajos Kossuth University, Debrecen, Hungary

1 Introduction

The partial width for the decay $Z^0 \rightarrow b\bar{b}$ is of special interest in the Standard Model. Electroweak corrections involving the top quark affect the $Z^0 \rightarrow b\bar{b}$ partial width, $\Gamma_{b\bar{b}}$, differently from the widths for lighter quarks. As a result, the fraction

$$\frac{\Gamma_{b\bar{b}}}{\Gamma_{\text{had}}} \equiv \frac{\Gamma(Z^0 \rightarrow b\bar{b})}{\Gamma(Z^0 \rightarrow \text{hadrons})}$$

depends on the top quark mass, m_{top} , but has negligible uncertainty from the unknown Higgs boson mass and the strong coupling constant α_s . The fraction $\Gamma_{b\bar{b}}/\Gamma_{\text{had}}$ is also sensitive to various extensions of the Standard Model involving new particles such as additional quarks and gauge bosons, or the virtual effects of new scalars and fermions such as those expected in supersymmetric models [1].

This paper describes an update of the previously published OPAL measurement [2] of the fraction of $b\bar{b}$ events in hadronic Z^0 decays. The measurement method remains largely unchanged in this update, while the data statistics are approximately doubled by including the data collected in 1994. In this paper we discuss only the most important features of the measurement, concentrating on changes from the previous paper [2].

The quantity measured in the analysis is the cross-section ratio

$$R_b \equiv \frac{\sigma(e^+e^- \rightarrow b\bar{b})}{\sigma(e^+e^- \rightarrow \text{hadrons})}$$

at the Z^0 resonance. This differs from the partial width ratio $\Gamma_{b\bar{b}}/\Gamma_{\text{had}}$ because of the additional contribution from photon-exchange diagrams. These have been evaluated within the Standard Model using the program ZFITTER [3]; their effect is to reduce R_b by 0.0003 compared to $\Gamma_{b\bar{b}}/\Gamma_{\text{had}}$. As in previous OPAL publications, this correction is not applied to the result in this paper. Note that the small number of $b\bar{b}$ pairs produced in the fragmentation process, rather than directly from Z^0 decays, are not included in the numerators of the definitions of $\Gamma_{b\bar{b}}/\Gamma_{\text{had}}$ and R_b .

In the measurement, two tagging methods are used to enrich the hadronic sample in $b\bar{b}$ events: one is to detect electrons or muons coming from semileptonic decays of bottom hadrons; the other is to find decay vertices of bottom hadrons separated significantly from the primary interaction point. The systematic error is kept low by the use of the double tagging technique, in which the tagging methods are applied to the two thrust hemispheres of each event, allowing the b tagging efficiency in a hemisphere, ϵ^b , to be calculated from the data by comparing the number of tagged hemispheres and the number of events with both hemispheres tagged.

The most important change in the analysis from the previous publication is in the treatment of the correlation of tagging efficiencies between the two event hemispheres. Studies using large samples of Monte Carlo simulated events have provided a better understanding of the origins of the efficiency correlation, resulting in slight modifications to the way the effects are evaluated. For the types of correlation effects that may not be well modelled by the simulation, for example the correlation between the momenta of the two b hadrons in a $b\bar{b}$ event due to final state QCD radiation, distributions of variables that are closely related to the correlation are compared between the real and simulated event samples. The size of the efficiency correlation and its systematic uncertainty presented in this paper are less dependent on any particular Monte Carlo event generator, and thus more reliable, than the previous estimate.

The principle of the double tagging technique is described in the next section. The most important features of the OPAL detector relevant to the analysis are described in Section 3. Section 4 reviews the event samples used, both from data and from simulation. The methods of tagging $b\bar{b}$ events using

leptons or secondary vertices are discussed in Section 5. The effect of the tagging efficiency correlation is discussed in Section 6. Section 7 presents the result of the R_b measurement. The estimation of the systematic errors on the measurement is described in Section 8.

2 Analysis Method

Each hadronic Z^0 decay event is divided into two hemispheres by the plane perpendicular to the thrust axis. A hemisphere is said to be *tagged* if it is selected by either of the two b-tagging methods, lepton tagging and vertex tagging, which are described in Section 5. The number of tagged hemispheres, N_t , and the number of events with two tagged hemispheres, N_{tt} , are counted in a sample of N_{had} hadronic events. Assuming no correlation between the tagging efficiencies of the two hemispheres in a given event (apart from the underlying flavour dependence), and assuming equal tagging probabilities for $u\bar{u}$, $d\bar{d}$ and $s\bar{s}$ events, the numbers N_t and N_{tt} can be expressed as

$$N_t = 2N_{\text{had}} \left\{ \varepsilon^b R_b + \varepsilon^c R_c + \varepsilon^{\text{uds}}(1 - R_b - R_c) \right\}, \quad (1)$$

$$N_{tt} = N_{\text{had}} \left\{ (\varepsilon^b)^2 R_b + (\varepsilon^c)^2 R_c + (\varepsilon^{\text{uds}})^2(1 - R_b - R_c) \right\}, \quad (2)$$

where ε^b , ε^c and ε^{uds} are the tagging efficiencies for hemispheres in $b\bar{b}$, $c\bar{c}$ and other flavours of events, respectively.

The tagging methods are designed to ensure that the efficiency ε^b for $b\bar{b}$ events is much larger than the efficiencies ε^c and ε^{uds} for light quark events. Neglecting the contribution from light quark events, the cross-section ratio R_b and the efficiency ε^b are obtained approximately by

$$R_b \approx \frac{N_t^2}{4N_{tt}N_{\text{had}}}, \quad (3)$$

$$\varepsilon^b \approx \frac{2N_{tt}}{N_t}. \quad (4)$$

Whereas ε^b can be obtained from the data themselves, the tagging probabilities ε^c and ε^{uds} have to be estimated with Monte Carlo simulation, which introduces systematic uncertainties. Since the contribution from light quarks gives only a small correction to the measurement, the systematic error from this method is small compared with measurements that rely on Monte Carlo simulation for predicting the bottom quark efficiency ε^b .

Equations (1) and (2) assume that the tagging efficiencies of the two hemispheres in an event are correlated only through the flavour of the primary quark pair. This assumption is not strictly valid, as there is a small efficiency correlation between hemispheres of a given flavour for physical and instrumental reasons. The effect of this efficiency correlation can be included by modifying equation (2) as

$$N_{tt} = N_{\text{had}} \left\{ C_b(\varepsilon^b)^2 R_b + C_c(\varepsilon^c)^2 R_c + C_{\text{uds}}(\varepsilon^{\text{uds}})^2(1 - R_b - R_c) \right\}, \quad (5)$$

where C_b , C_c and C_{uds} are the correlation factors for $b\bar{b}$, $c\bar{c}$ and other flavours of events, respectively. A correlation factor of greater (less) than unity means a positive (negative) correlation. Correlations in light flavour events have a negligible effect because the double-tagging efficiencies for these events are very small; the correlation factors are therefore set to

$$C_c = C_{\text{uds}} = 1 \quad (6)$$

in this analysis. The approximate solution for R_b becomes

$$R_b \approx \frac{C_b N_t^2}{4N_{tt}N_{\text{had}}}, \quad (7)$$

i.e. the result is proportional to the correlation factor C_b . An accurate knowledge of C_b is therefore vital for this measurement.

3 The OPAL Detector

The OPAL detector has been described in Reference [4], and only the components important for this analysis are reviewed here. The OPAL coordinate system is a right-handed orthonormal system with its origin at the geometrical centre of the detector. The positive z axis lies along the electron beam direction and θ and ϕ are the polar and azimuthal angles, respectively. The x direction points towards the centre of the LEP ring and the y direction points upwards.

The central tracking detectors consist of a silicon microvertex detector, a precision vertex drift chamber, a large volume jet chamber, and thin surrounding z -chambers. The silicon microvertex detectors [5, 6] relevant to the data used in this analysis consisted of two layers of silicon microstrip detectors, one at a radius of 6.1 cm with an angular coverage of $|\cos\theta| < 0.83$ and one at a radius of 7.5 cm with an angular coverage of $|\cos\theta| < 0.77$. The microvertex detector can provide two measurements of the ϕ position for each track with an effective positional resolution of about 10 μm . The silicon microvertex detector was upgraded [6] before the 1993 data-taking to provide in addition up to two measurements of the z position of each track, but only the ϕ information was used for this analysis. When combined with angle and curvature information provided by the other central detector components, the r - ϕ impact parameter resolution for $Z^0 \rightarrow \mu^+\mu^-$ and $Z^0 \rightarrow e^+e^-$ events is 18 μm . The vertex detector is a high resolution drift chamber with axial and stereo wires. The jet chamber, approximately 4 m long and 3.7 m in diameter, provides up to 159 space points per track, and measures the ionization energy loss of charged particles [7]. The z coordinates of jet chamber hits are determined using charge division. The precision of the determination of track polar angles is improved by the z -chambers, which provide up to six measurements of the z coordinate on each track. The whole central tracking detector is surrounded by a solenoidal coil which provides a uniform magnetic field of 0.435 T. For the combined central detector, the resolution $\sigma(p_{xy})$ of the momentum in the bending plane of the magnetic field is given by $\sigma(p_{xy})/p_{xy} = \sqrt{(0.02)^2 + (0.0015p_{xy})^2}$ for p_{xy} in GeV/ c . The average resolution of the azimuthal track angle is 0.25 mrad. The polar angle resolution varies from 2 mrad for tracks with z -chamber hits to 20 mrad for tracks without them. In multihadronic events, the ionization energy loss measurement has a resolution of 3.5% for tracks with 159 samples.

A lead-glass electromagnetic calorimeter surrounds the magnet coil. The calorimeter is divided into a cylindrical barrel, covering the polar angle range $|\cos\theta| < 0.82$, and annular endcaps, covering the range $0.81 < |\cos\theta| < 0.98$. The barrel calorimeter consists of 9440 lead-glass blocks arranged in a nearly projective geometry. The energy resolution σ_E of the barrel electromagnetic calorimeter is approximately $\sigma_E/E \simeq 2.3\%$ for beam-momentum electrons from $e^+e^- \rightarrow e^+e^-$ events. The resolution on the ratio of the energy to momentum for electrons with energies between 2 and 3 GeV has been measured to be $\sigma(E/p) \approx 10.5\%$ using $e^+e^- \rightarrow e^+e^-\gamma$ events.

Outside the electromagnetic calorimeter lies the iron return yoke of the magnet, instrumented with streamer tubes as a hadron calorimeter. The muon detectors are placed outside the hadron calorimeter. In total at least 7, and in most regions 8, absorption lengths of material lie between the interaction point and the muon detectors. Muons with momenta above 3 GeV/ c usually penetrate to the muon detectors. The chambers are constructed as two different detector subsystems in the barrel and endcap parts of the detector. The muon barrel detector covers the polar angle range $|\cos\theta| < 0.7$. It has a cylindrical geometry, composed of four layers of planar chambers staggered to resolve left-right ambiguities. The chambers provide coordinate measurements with an accuracy of 1.5 mm in r - ϕ , and 2 mm in z . The muon endcap detector covers the polar angle range $0.67 < |\cos\theta| < 0.98$. It consists of two separated planes of limited streamer tube arrays at each end of the OPAL detector. Resolutions

of 1–3 mm are obtained on the x and y coordinates of hits using the sharing of charge between strips, and the z coordinate is obtained from the surveyed positions of the chambers.

4 Hadronic Event Selection

The data used for this analysis were collected from e^+e^- collisions at LEP during 1992, 1993 and 1994, with centre-of-mass energy at and around the peak of the Z^0 resonance. Hadronic Z^0 events were selected using an algorithm described in Reference [8], additionally requiring that there be at least seven charged tracks in each event. The hadronic Z^0 event selection efficiency is $(98.1 \pm 0.5)\%$, with a background of less than 0.1%.

The thrust value and the direction of the thrust axis of each hadronic event were calculated using charged tracks together with electromagnetic clusters with no associated tracks. Two additional cuts were applied to each event: the thrust value, T , must be at least 0.8, and the polar angle of the thrust axis, θ_{thrust} , must satisfy $|\cos \theta_{\text{thrust}}| < 0.7$. These cuts were designed to ensure good definition of the thrust direction and to match the acceptance of the silicon microvertex detector.

A total of 1517282 hadronic events passed the event selection. The data samples collected in different years were analysed independently because the tagging efficiencies were expected to be slightly different due to small variations in the detector performance. The data collected in 1994 were all taken at centre-of-mass energies, E_{cm} , very close to the peak of the Z^0 resonance, and account for 51% of the data sample. The data taken in 1993 at energies above or below the peak of the resonance have been included, as in the previously published analysis, since they are expected to have almost the same $b\bar{b}$ fraction and tagging efficiency. Of the total, 3.2% of the hadronic events were recorded at $E_{\text{cm}} = 89.45$ GeV, and 4.7% at $E_{\text{cm}} = 93.04$ GeV, where the values of R_b calculated by ZFITTER [3] are lower than the value at the Z^0 peak by -0.00075 and -0.00040 , respectively. The impact of including these off-peak data samples is therefore to reduce the measured value of R_b by -0.00004 . This correction is not applied to the measurement of R_b presented here.

The background in the event selection is dominated by $e^+e^- \rightarrow \tau^+\tau^-$ events, which constitute about 0.065% of the selected events. These background events have a very low probability of being tagged as $b\bar{b}$ candidates. Their effect on the R_b measurement is therefore to increase the total number of events by 0.065%, thereby decreasing the measured value of R_b by the same fraction.

The event selection was designed to have the same acceptance for any quark flavour. There is, however, a small flavour bias caused by the charged track multiplicity requirement: bottom quark events have a higher average multiplicity, and hence a higher efficiency, than the other flavours. This flavour bias increases the value of R_b in the selected event sample relatively by 0.32%. Combined with the effect of the tau-pair background, a relative correction of $(-0.25 \pm 0.15)\%$ has to be applied to the measured value of R_b , where the error is due to the uncertainty in the simulation of the track multiplicity distribution and to Monte Carlo statistics.

Charged tracks and electromagnetic calorimeter clusters with no associated track were combined into jets using the JADE algorithm [9] with the E0 recombination scheme [10]. The invariant mass-squared cut-off was set to $x_{\text{min}} = 49 (\text{GeV}/c^2)^2$. The transverse momentum, p_t , of each track was defined relative to the axis of the jet containing it, where the jet axis was calculated including the momentum of the track.

Monte Carlo simulated events were used for evaluating backgrounds, acceptances for light quark events, and efficiency correlations between the two hemispheres of an event. Hadronic events were simulated with the JETSET 7.4 Monte Carlo event generator [11] in conjunction with a program that modelled the response of the OPAL detector [12]. All simulated events were generated with a centre-of-mass energy corresponding to the Z^0 resonance. The tagging efficiencies predicted by the

simulation were corrected for the known changes in the configuration and operating condition of the OPAL detector during the data-taking period.

The parameters used in JETSET were optimised by OPAL [13]. The fragmentation function of Peterson et al. [14] was used to describe the fragmentation of b and c quarks. The tagging probabilities for light-quark events, ε^c and ε^{uds} , are sensitive to the following input parameters:

- the average semileptonic branching fractions for the charmed hadrons,
- the momentum spectra of the leptons in the rest frame of the decaying charmed hadrons,
- the production fractions of the weakly decaying charmed hadrons in $c\bar{c}$ events,
- the lifetimes of the charmed hadrons,
- the average charged decay multiplicities of the charmed hadrons,
- the production rates of b and c quarks via gluon splitting, and
- the production rates of K^0 's and hyperons.

These parameters were tuned in the JETSET Monte Carlo to reflect the most up-to-date measurements. The central values of the parameters and their uncertainties used in evaluating the systematic error are given in Section 8.

5 b Tagging

For each multihadronic event, two methods of tagging $b\bar{b}$ events were applied independently to each of the two hemispheres: lepton tagging and vertex tagging. The vertex tag carries a greater weight in the analysis, having both higher b tagging efficiency and smaller background than the lepton tag.

5.1 Lepton Tagging

Leptons with high momentum, p , and a large momentum component transverse to the jet axis, p_t , are expected to come mainly from semileptonic decays of b hadrons, because of the hard fragmentation and the large mass of the b quark. Electrons with $p > 2 \text{ GeV}/c$ and $p_t > 1.1 \text{ GeV}/c$, and muons with $p > 3 \text{ GeV}/c$ and $p_t > 1.2 \text{ GeV}/c$ were used in this analysis to tag $b\bar{b}$ event candidates, and were identified using the algorithms described in References [15] and [16], respectively.

Electron candidates were selected in the barrel region of the detector, $|\cos\theta| < 0.715$. Identification of electrons relies on the ionisation energy loss, dE/dx , measured in the tracking chamber and on the total absorption of the energy in the electromagnetic calorimeter. Candidates were rejected if they were consistent with coming from a photon conversion when paired with an oppositely charged track in the same event. The expected identification efficiency for electrons from decays of bottom hadrons in the kinematical acceptance is about 68%.

A total of 19555 hemispheres were tagged by electrons after the photon conversion rejection. The number of electrons coming from photon conversions which escaped the rejection was estimated to be 382 ± 143 based on the performance of the rejection algorithm predicted by the Monte Carlo. The hadronic background in the sample was estimated to be 1647 ± 153 candidates using the distribution of the identifying variables measured in the data. The methods used for estimating these backgrounds and their systematic errors are described in more detail in Reference [15].

Muon candidates were selected in a polar angle range $|\cos\theta| < 0.9$. Identification of muons relied on their ability to penetrate material. Track segments reconstructed in the four-layer external muon chambers were matched to the tracks extrapolated from the central tracking detectors. The presence of a matching segment and the quality of the positional match were used to identify muons. The measured dE/dx was also required to be consistent with a muon. The expected identification efficiency for muons from decays of bottom hadrons in the kinematical acceptance is about 75%.

A total of 22248 hemispheres containing muon candidates were found in the data. The background in the selected muon sample was estimated to be 2577 ± 220 candidates using the misidentification probability predicted by the Monte Carlo. A detailed description of the systematic error estimation can be found in Reference [16].

5.2 Vertex Tagging

Hadronic Z^0 decays into bottom quarks can be enriched by taking advantage of the relatively long (~ 1.5 ps) lifetimes of bottom hadrons. In this analysis, the detection of secondary vertices significantly separated from the primary vertex was adopted to exploit this long lifetime.

The primary vertex for each event was reconstructed by fitting all good tracks in the event to a common point in the x - y plane, incorporating a constraint from the average beam spot position and uncertainty derived from the data. The typical size of the beam spot observed by the detector, including the uncertainty due to the detector resolution, is 100–150 μm in x and 5–20 μm in y depending on the data-taking period. Tracks with a large χ^2 contribution to the fit were removed one by one, until all remaining tracks contributed less than 4 to the χ^2 . In about 0.1% of the events, no tracks remained after this procedure, in which case the average beam spot position was used as the primary vertex.

For each jet, a secondary vertex was sought by fitting the charged tracks passing a set of track quality criteria to a common point in the x - y plane. Each track used in the fit was required to have a momentum greater than 500 MeV/ c , a distance of closest approach $|d_0|$ in the x - y plane to the primary vertex smaller than 0.3 cm, and an error σ_{d_0} smaller than 0.1 cm. Tracks with a large χ^2 contribution to the fit were removed one by one, until all remaining tracks contributed less than 4 to the χ^2 . In a b jet, because of the large average track multiplicity of b hadron decays and the hard fragmentation of the b quark, the tracks retained by the algorithm are more likely to be those from the b hadron decay. At least four tracks were required to remain in the fit for the secondary vertex finding to be successful for the jet.

The vertex decay length L was defined as the distance of the secondary vertex from the primary vertex in the plane transverse to the beam direction, constrained by the direction of the total momentum vector of the tracks assigned to the secondary vertex. The total vertex momentum vector was also used to determine the sign of the decay length; $L > 0$ if the secondary vertex was displaced from the primary vertex in the same direction as the total momentum, and $L < 0$ otherwise.

Each event hemisphere was assigned a forward and/or a backward vertex tag based on the signed decay length significance, defined as the signed decay length L divided by its error σ_L , of the secondary vertices it contained. Hemispheres containing a secondary vertex with $L/\sigma_L > 8$ are forward tagged, and those with a secondary vertex with $L/\sigma_L < -8$ are backward tagged. Forward tags enrich the $b\bar{b}$ fraction of the sample, while the backward tags were used to control the systematics associated with the detector resolution.

The decay length significance L/σ_L is an inherently symmetric variable: its distribution should be symmetric about $L/\sigma_L = 0$ if there are no particles with detectable lifetime. For light quark events, any change in the detector resolution is expected to increase or decrease the fractions of forward and backward tags by similar amounts, but their difference will be relatively insensitive to such a change.

Equations (1) and (5) can be modified, or *folded*, so that they contain only the difference between the forward and the backward tagging efficiencies:

$$N_v - N_{\bar{v}} = 2N_{\text{had}} \left\{ (\varepsilon_v^b - \varepsilon_{\bar{v}}^b) R_b + (\varepsilon_v^c - \varepsilon_{\bar{v}}^c) R_c + (\varepsilon_v^{\text{uds}} - \varepsilon_{\bar{v}}^{\text{uds}}) (1 - R_b - R_c) \right\}, \quad (8)$$

$$N_{vv} - N_{v\bar{v}} + N_{\bar{v}\bar{v}} = N_{\text{had}} \left\{ C_b (\varepsilon_v^b - \varepsilon_{\bar{v}}^b)^2 R_b + (\varepsilon_v^c - \varepsilon_{\bar{v}}^c)^2 R_c + (\varepsilon_v^{\text{uds}} - \varepsilon_{\bar{v}}^{\text{uds}})^2 (1 - R_b - R_c) \right\}, \quad (9)$$

where the five quantities on the left-hand side are

- N_v the number of forward tagged hemispheres,
- $N_{\bar{v}}$ the number of backward tagged hemispheres,
- N_{vv} the number of events for which both hemispheres receive a forward tag,
- $N_{\bar{v}\bar{v}}$ the number of events for which both hemispheres receive a backward tag,
- $N_{v\bar{v}}$ the number of events for which one hemisphere receives a forward tag and the other a backward tag.

The efficiencies ε_v^b , $\varepsilon_{\bar{v}}^c$ and $\varepsilon_v^{\text{uds}}$ are defined as the probabilities of obtaining a forward vertex tag in a hemisphere in $b\bar{b}$, $c\bar{c}$ and other light quark events, respectively, and $\varepsilon_{\bar{v}}^b$, $\varepsilon_{\bar{v}}^c$ and $\varepsilon_{\bar{v}}^{\text{uds}}$ are the corresponding probabilities for a backward vertex tag. The *folded double tagging* measurement can then be carried out following a similar procedure to that given in Section 2, except that now equations (8) and (9) are solved for the two unknowns $(\varepsilon_v^b - \varepsilon_{\bar{v}}^b)$ and R_b . In place of the light flavour tagging efficiencies ε^c and ε^{uds} , the differences of the forward and backward tagging probabilities $(\varepsilon_v^c - \varepsilon_{\bar{v}}^c)$ and $(\varepsilon_v^{\text{uds}} - \varepsilon_{\bar{v}}^{\text{uds}})$ need to be estimated from Monte Carlo simulation. This results in a measurement more robust against the uncertainty in the detector resolution. We note that, in practice, the backward efficiency for $b\bar{b}$ events, $\varepsilon_{\bar{v}}^b$, is much smaller than the forward efficiency ε_v^b so that $(\varepsilon_v^b - \varepsilon_{\bar{v}}^b)$ is nearly equal to ε_v^b .

Figure 1(a) shows the inclusive L/σ_L distribution for secondary vertices reconstructed in the 1994 data sample, and in Monte Carlo events. Vertices with large positive values of L/σ_L are dominantly produced in $b\bar{b}$ events. The Monte Carlo provides a good description of the data in this region, though this is not essential for this analysis because the b quark tagging efficiency is measured from the data.

Differences between data and Monte Carlo are seen in the region around $L/\sigma_L = 0$ and in the backward half ($L/\sigma_L < 0$) of the decay length distribution. These differences are due largely to an over-optimistic simulation of the detector resolution and hit-association probabilities for charged tracks. The resolution in the Monte Carlo was therefore degraded in order to improve the agreement between data and Monte Carlo. This was done by applying a single multiplicative scaling factor, β , to the difference between the reconstructed and true track impact parameters and ϕ angle measurements. The L/σ_L distribution using a scaling factor $\beta = 1.1$ is shown in Figure 1(b) and is seen to give a much improved description of the data.

Figure 2 shows the dependence on the resolution scaling factor β of the fractions f_v ($f_{\bar{v}}$) of hemispheres in the Monte Carlo containing a forward (backward) vertex tag. The horizontal bands indicate the tagging fractions measured in the 1994 data, with their associated statistical errors. The backward tagging fraction $f_{\bar{v}}$ is primarily determined by the resolution of the detector, and agreement of this quantity between data and Monte Carlo can be used to determine the value of β . A central value $\beta = 1.1$ was used for this analysis, and a variation from $\beta = 1.0$ (i.e. no resolution degradation) to $\beta = 1.4$ was used to estimate the systematic error due to uncertainties in the modelling of the detector resolution. The resulting systematic error on the measured value of R_b will be discussed in

Section 8. The central value of the resolution scaling factor needed here, i.e. $\beta = 1.1$, is smaller than the value $\beta = 1.4$ used in the previously published measurement [2], mainly due to improvements in the simulation of the jet and vertex drift chamber resolutions in the Monte Carlo.

The forward and backward tagging efficiencies, $\varepsilon_v^{\text{uds}}$ and $\varepsilon_{\overline{v}}^{\text{uds}}$, and their difference for Monte Carlo $Z^0 \rightarrow u\overline{u}, d\overline{d}, s\overline{s}$ events are shown in Figure 3 as a function of the scaling factor β . A similar plot for the charm tagging efficiencies is shown in Figure 4. In both cases, the forward and backward tagging efficiencies rise significantly as the resolution in the Monte Carlo is degraded, but the folded tagging efficiencies remain rather stable. The sensitivity of the predicted tagging efficiencies to the modelling of the silicon microvertex hit association efficiency and alignment precision was also studied in the Monte Carlo, by varying the fraction of tracks with associated silicon hits and by changing the radial positions of the silicon ladders. In each case, the folded tagging efficiencies $\varepsilon_v^{\text{uds}} - \varepsilon_{\overline{v}}^{\text{uds}}$ and $\varepsilon_v^c - \varepsilon_{\overline{v}}^c$ were found to be insensitive to these variations.

After correcting for a known difference in the coverage of the silicon microvertex detector, the fraction of hemispheres tagged by a forward vertex was found to be $(0.10 \pm 0.03)\%$ higher in the 1994 data than in the earlier data samples (a relative increase of 2.2%). This change is attributed to improvements in the quality of the detector calibration and alignment in the later data. For example, the fraction of tracks with at least one associated silicon microvertex hit was 1.0% higher in the 1994 data, while the fraction of tracks with associated vertex chamber hits was 1.8% higher. The change in the forward tagging efficiency predicted by the Monte Carlo as the resolution scaling factor was varied between $\beta = 1.0$ and $\beta = 1.4$, shown in Figure 2, is larger than the difference observed between the 1994 and earlier data samples. No significant change in the fraction of hemispheres with a backward vertex tag is observed for the different years of data taking, whereas from Figure 2, a slight decrease in the backward tagging fraction might be expected for the later data. Within the statistical precision, however, the behaviour of the backward tagging fraction in the data is consistent with that observed in the Monte Carlo by varying the scaling factor β . The range of uncertainty allowed in the scaling factor β is therefore sufficient to cover the uncertainty due to the detector calibration and alignment.

The fraction of double-tagged events, where both hemispheres contain a forward vertex tag, was also found to be higher in the 1994 data. The measured values of R_b , given approximately by equation (3), were found to be consistent for the 1992, 1993 and 1994 data samples. No significant variation was observed for different periods of data taking within each year of data. The dependence of the R_b measurement on the spatial (θ and ϕ) direction of the event thrust axis was also studied, and no significant variations were observed.

It is important to note that the vertex tagging algorithm adopted in this analysis has been chosen because it is relatively insensitive to the resolution with which the primary vertex is reconstructed. The primary vertex is used only in the calculation of the decay length L ; the secondary vertex finding is carried out completely independently of the primary vertex, apart from the loose requirement on $|d_0|$ of the tracks used. The primary vertex has an average error of about $40 \mu\text{m}$ along the direction of the event thrust axis, while the typical error σ_L on the decay length L for b hadrons near the forward-tag threshold ($L/\sigma_L = 8$) is about $300 \mu\text{m}$. The measured decay length significance, and thus the vertex tagging efficiency, is therefore only weakly affected by the resolution of the primary vertex reconstruction. This keeps the efficiency correlation between the two hemispheres of an event, and its uncertainty, small, as will be shown in Section 6.1. It is possible to achieve a better b-quark efficiency and better light-quark rejection by using tagging algorithms that rely more heavily on the primary vertex. Such algorithms, however, would potentially introduce a strong hemisphere-hemisphere efficiency correlation through the primary vertex shared by both hemispheres.

6 Efficiency Correlation

The assumption that the hemisphere tagging probabilities for the two hemispheres of an event are correlated only through the flavour of the initial quark pair is not perfectly correct. Hemisphere efficiency correlations can arise from the following three origins: (1) correlations coming from the determination of the primary vertex, (2) kinematical correlations due to final state QCD radiation, and (3) geometrical correlations due to detector non-uniformities.

The efficiency correlation, C_b , can be obtained from simulated $b\bar{b}$ events by measuring the ratio of the double-tagging probability to the square of the hemisphere tagging probability. The accuracy of such an estimate is limited by the statistics of the Monte Carlo sample as well as by any inadequacy of the simulation. Therefore, in this measurement, an alternative approach to estimating the correlation was used. The hemisphere efficiency correlation was divided into contributions from the three origins above, which were estimated separately either from the data or using the Monte Carlo simulation. Where possible, distributions of the variables that are related to the origin of the correlation were compared between the real and simulated data to estimate the systematic error. In cases where no such comparison is possible, systematic errors were assessed by varying the input parameters to which the Monte Carlo simulation is expected to be sensitive. The total correlation was obtained by adding up the separate contributions. Possible interdependences between different origins of correlation were considered and included in the systematic errors. The validity of the procedure was tested using a large sample of Monte Carlo $b\bar{b}$ events generated using a fast detector simulation.

The hemisphere efficiency correlation values quoted in this section refer to the combined tag, which requires either a secondary vertex or a lepton in an event hemisphere to be tagged. The efficiency correlation for the lepton and vertex tags separately has also been evaluated and will be summarised below in Table 1.

6.1 Primary Vertex Correlation

The position of the primary vertex is determined in each event by fitting the tracks in the whole event to a common point, with an additional constraint derived from the knowledge of the LEP beam spot. The primary vertex position and its error are used for vertex tagging in both hemispheres and hence can be a source of efficiency correlation.

Since the majority of $b\bar{b}$ events have two b hadrons directed approximately back-to-back along the direction of the event thrust axis, any displacement of the measured primary vertex from the true position causes negatively correlated changes in the measured decay lengths in the two event hemispheres. In addition, the size of the estimated error of the vertex position, which varies from event to event, contributes to the measurement error on the decay length in both hemispheres, giving a positive correlation. The size of the correlation expected from this naive picture is, however, very small ($|C_b - 1| < 0.1\%$) because the tagging efficiency depends only weakly on the primary vertex position and error as discussed in Section 5.2.

An efficiency correlation in fact arises mainly because the primary vertex fitting may also include tracks coming from b hadron decays. This makes the primary vertex position biased towards the direction of flight of the b hadron, and also reduces the estimated error from the primary vertex fitting because a larger number of tracks are used. The position bias and the reduction of the error occur especially when the true b hadron decay length is short, i.e. when the tagging efficiency in the hemisphere is low. At the same time, both effects tend to increase the tagging efficiency in the other hemisphere; thus the position and error both give rise to negative efficiency correlations.

The effect of the primary vertex reconstruction can be isolated in the Monte Carlo by replacing the measured primary vertex position with the true one, and reducing the measurement error to zero.

The size of the correlation was estimated in a sample of 1 million Monte Carlo $b\bar{b}$ events by evaluating the change in the value of the overall correlation when the primary vertex was modified in this way. This gave $C_b - 1 = (-0.47 \pm 0.13)\%$ for the combined tag requiring either a secondary vertex or a lepton in an event hemisphere, where the error is due to the Monte Carlo statistics.

The correlation prediction relies on a good knowledge of the detector tracking resolution, the LEP beam spot size, the b quark fragmentation, the b hadron lifetimes and the charged decay multiplicities. The systematic error was estimated by varying each of these inputs as follows:

Detector Resolution: The resolution of the detector was varied in the Monte Carlo using the method discussed in Section 5.2. No systematic trend was observed for variations of the scaling factor β within the range 1.0–1.4. The largest difference observed in $C_b - 1$, 0.14%, was taken as the systematic error.

Beam spot size: The average size of the LEP beam spot varied between the data taking periods; for example, the r.m.s. spread of the beam spot in the horizontal plane was about $100 \mu\text{m}$ in 1992 and about $150 \mu\text{m}$ in 1993. The beam spot size was effectively varied in the Monte Carlo so that the range of the variation covers the beam spot sizes measured in all data samples used in this analysis. This was achieved by varying the position and the uncertainty of the beam spot constraint used in the primary vertex fitting for each event. A systematic variation of $\pm 0.06\%$ was observed in $C_b - 1$ as the horizontal beam spot size was varied between $100 \mu\text{m}$ and $160 \mu\text{m}$. The effect on $C_b - 1$ of varying the vertical beam spot size was found to be less than 0.01% and was neglected.

Bottom quark fragmentation: The b quark fragmentation was varied by applying a weight to each simulated event using the fragmentation function of Peterson et al. [14] so that the average scaled energy of the weakly-decaying b hadron, $\langle x_E \rangle_b$, changed by ± 0.008 . The range of the variation reflects the accuracy of $\langle x_E \rangle_b$ measured by LEP experiments [15,17]. The observed variation in $C_b - 1$, $\pm 0.03\%$, was taken as the systematic error.

Bottom hadron lifetime: The lifetimes of the b hadrons were varied simultaneously by ± 0.05 ps using a weighting method. The size of the variation was chosen to be larger than the accuracy of the world average [18] to allow for the uncertainty due to different efficiencies for different b hadron species. The observed variation in $C_b - 1$ was smaller than the uncertainty due to the Monte Carlo statistics, $\pm 0.01\%$, and the latter was taken as the systematic error.

Bottom charged decay multiplicity: The average charged decay multiplicity of the b hadrons was varied by ± 0.35 using a weighting method. The size of the variation reflects the accuracy of the measurements by OPAL [19] and DELPHI [20]. The observed variation in $C_b - 1$, $\pm 0.04\%$, was taken as the systematic error.

Adding these errors and the Monte Carlo statistical error in quadrature, $C_b - 1 = (-0.47 \pm 0.21)\%$ was obtained as the estimated correlation due to the primary vertex reconstruction.

6.2 Kinematical Correlation

The hadronic decay of a Z^0 may produce one or more gluons carrying a substantial amount of energy. In such an event, there is less energy available for the primary quark pair, thus resulting in smaller chances of the b and \bar{b} hemispheres being tagged by high momentum leptons or by displaced vertices. A positive correlation is expected from this effect. In addition, in the presence of hard gluon jets, the b and \bar{b} can be produced in the same event hemisphere, which will be seen to lead to a small effective negative correlation.

6.2.1 Same-hemisphere events

The JETSET Monte Carlo predicts that 1.21% of $b\bar{b}$ events passing the event selection have both bottom hadrons in one thrust hemisphere. These same-hemisphere $b\bar{b}$ events represent only 0.66% of all tagged hemispheres because of the lower tagging efficiency of such events. As these events contribute to only 0.02% of the double-tagged event sample, they effectively decrease the double-tagging efficiency by $(1.21 - 0.02)\%$ and the single-tagging efficiency by $(1.21 - 0.66)\%$. The correlation factor C_b is given by dividing the double-tagging efficiency by the single-tagging efficiency squared, and these efficiency changes therefore introduce a hemisphere correlation of approximately

$$C_b - 1 = -(1.21 - 0.02)\% + 2(1.21 - 0.66)\% = (-0.09 \pm 0.04)\%,$$

where the error is due to Monte Carlo statistics. The size of the effect was found to be stable to within $\pm 0.02\%$ by using true primary vertices in place of measured ones, and extending the definition of same-hemisphere events by allowing b hadrons near the hemisphere boundary to belong to both sides of the event.

The rate of same-hemisphere events was compared between the data and the Monte Carlo simulation by looking for events with two vertex-tagged jets in one hemisphere. A loose vertex tag requiring the decay length significance $L/\sigma_L > 4$ was used to improve the statistics of the test. Approximately 30% of such double-tagged hemispheres come from real same-hemisphere $b\bar{b}$ events, about 60% from normal $b\bar{b}$ events with a misreconstructed vertex, and 10% from light quark events. These contributions can be statistically separated using the three-dimensional angle, φ_{vv} , between the momentum vectors of the two vertices. The signal has a broad φ_{vv} distribution, as shown in Figure 5, while the backgrounds are concentrated near $\varphi_{vv} = 0$. The φ_{vv} distribution obtained from the data was fitted to the sum of the Monte Carlo distributions for the three components, allowing the normalisations to vary. The fit was repeated with and without the requirement that the events pass the thrust value cut ($T > 0.8$). Removing the thrust value cut increases the number of same-hemisphere events significantly, thereby making a more sensitive test of the effect. The rate of double-tagged hemispheres from same-hemisphere $b\bar{b}$ events obtained from the fit was found to be consistent with the Monte Carlo prediction within an uncertainty of $\pm 11\%$. Varying the rate of same-hemisphere $b\bar{b}$ events and the tagging efficiency for them independently by $\pm 11\%$ in the Monte Carlo resulted in a systematic uncertainty of $\pm 0.15\%$ on the predicted value of C_b . Including the Monte Carlo statistical error, the effect of the same-hemisphere $b\bar{b}$ events was estimated to be $C_b - 1 = (-0.09 \pm 0.16)\%$.

6.2.2 Momentum correlations

After removing same-hemisphere events, each hemisphere of a $b\bar{b}$ event contains one b hadron. The tagging efficiency ε^b for the hemisphere is a strong function of the momentum of the b hadron p_B , and the correlation of the two b hadron momenta, p_B and $p_{\bar{B}}$, produces an efficiency correlation. The size of the b hadron momentum correlation in a Monte Carlo sample can be characterised by

$$C_{p_B} \equiv \frac{\langle p_B p_{\bar{B}} \rangle}{\langle p_B \rangle \langle p_{\bar{B}} \rangle}, \quad (10)$$

where the average is calculated over all events in the sample. Using the tagging efficiency ε^b obtained from the Monte Carlo as a function of the bottom hadron momentum, the momentum correlation leads to an efficiency correlation

$$C_b = \frac{\langle \varepsilon^b(p_B) \varepsilon^b(p_{\bar{B}}) \rangle}{\langle \varepsilon^b(p_B) \rangle \langle \varepsilon^b(p_{\bar{B}}) \rangle}. \quad (11)$$

The JETSET Monte Carlo was found to predict a small positive b momentum correlation of $C_{p_B} - 1 = (+0.84 \pm 0.01)\%$ which translated to an efficiency correlation of $C_b - 1 = (+0.53 \pm 0.02)\%$ for the combined lepton and vertex tag, where the errors are due to the Monte Carlo statistics.

The tagging efficiency for a $b\bar{b}$ event hemisphere in the Monte Carlo was found to depend not only on the b hadron momentum in that hemisphere, as in equation (11), but also on the momentum of the b hadron in the opposite hemisphere. The b tagging efficiency is predicted to fall slightly as the b hadron momentum in the opposite hemisphere increases, giving rise to a negative efficiency correlation component which must be added to the positive p_B - $p_{\bar{B}}$ correlation component of equation (11).

This additional source of efficiency correlation was found to affect the vertex tag only, arising as an indirect consequence of the influence of the fragmentation tracks around the b hadron on the vertex tagging efficiency. The efficiency to reconstruct a secondary vertex in a b hemisphere depends primarily on the production and decay properties of the b hadron, but also on the number of fragmentation tracks in the hemisphere, N_{frag} . N_{frag} depends strongly on the momentum of the b hadron in the same hemisphere, decreasing as the b hadron momentum increases since less energy is available for the residual fragmentation of the b quark. In addition, however, N_{frag} is found to depend on the momentum of the b hadron in the opposite hemisphere. The net effect of the fragmentation tracks is therefore to introduce an indirect dependence of ε^b on the momentum of the b hadron in the other hemisphere, $p_{\bar{B}}$. In evaluating the efficiency correlation, C_b , the efficiency ε^b in equation (11) must therefore be parametrised as a function of both p_B and $p_{\bar{B}}$:

$$C_b = \frac{\langle \varepsilon^b(p_B, p_{\bar{B}}) \varepsilon^b(p_{\bar{B}}, p_B) \rangle}{\langle \varepsilon^b(p_B, p_{\bar{B}}) \rangle \langle \varepsilon^b(p_{\bar{B}}, p_B) \rangle}. \quad (12)$$

This equation includes both the p_B - $p_{\bar{B}}$ correlation and the effects of N_{frag} . The latter can be estimated by subtracting the correlation given by (11) from that given by (12).

Since the primary vertex resolution is strongly affected by N_{frag} , the correlation caused by N_{frag} and the correlation due to the primary vertex may be interdependent. Using Equation (12), the Monte Carlo predicted $C_b - 1 = (-0.03 \pm 0.04)\%$ when the measured primary vertex was used, and $(+0.06 \pm 0.04)\%$ with the true primary vertex. The latter is taken as the central value as it does not include the primary vertex effect, and the difference, 0.09%, is included in the systematic error when the total correlation is calculated. Subtracting the p_B - $p_{\bar{B}}$ effect of $(+0.53 \pm 0.02)\%$, which was found to be insensitive to the choice of the primary vertex, leaves $C_b - 1 = (-0.47 \pm 0.05)\%$ for the size of the N_{frag} effect.

The Monte Carlo predictions for the p_B - $p_{\bar{B}}$ correlation and the N_{frag} effect were tested using the data. The momentum of the lepton or the total momentum of the tracks assigned to the secondary vertex was studied for hemispheres with lepton or vertex tags, respectively, since these quantities are reasonably correlated with the b hadron momentum. In addition, the number of tracks in the hemisphere was used as an estimator of the number of fragmentation tracks. This is valid because the number of tracks from the b hadron decay, i.e. the difference between the number of tracks in a hemisphere and the number of fragmentation tracks, cannot be affected by $p_{\bar{B}}$, the momentum of the other b hadron.

The thresholds for the tags were chosen to maximise the statistical significance of the test, while keeping the effect of the light-quark background negligible. For the lepton tag, electrons or muons with transverse momenta greater than 0.8 GeV/c were accepted. For the vertex tag, the decay length significance L/σ_L was required to be larger than 4. Four measurements were performed on the data and on the Monte Carlo to test the two types of correlations:

- The p_B - $p_{\bar{B}}$ correlation was tested by measuring

- the correlation between the momenta of the vertices in events with two vertex tags, and
- the correlation between the lepton momentum and the vertex momentum in events with lepton and vertex tags in the opposite hemispheres;
- The N_{frag} effect was tested by measuring
 - the dependence of the average hemisphere track multiplicity on the momentum of the vertex in the other hemisphere, and
 - the dependence of the average hemisphere track multiplicity on the momentum of the lepton in the other hemisphere.

From these tests, the sizes of the p_B - $p_{\bar{B}}$ correlation and the correlation due to the N_{frag} effect were found to be consistent between the data and the JETSET Monte Carlo, within large statistical uncertainties of $\pm 40\%$ each. The effects on these comparisons of the light-flavour background and the same-hemisphere $b\bar{b}$ events were negligible according to the Monte Carlo. Allowing $\pm 40\%$ relative uncertainties on the values predicted by the Monte Carlo, the p_B - $p_{\bar{B}}$ and N_{frag} correlations in the data were estimated to be $C_b - 1 = (+0.53 \pm 0.21)\%$ and $(-0.47 \pm 0.19)\%$, respectively. The quoted errors also include the Monte Carlo statistics.

In total, the kinematical correlation was estimated to be $C_b - 1 = (-0.03 \pm 0.33)\%$, where the error comes mainly from the statistical precision of the comparisons between the data and the Monte Carlo.

6.3 Geometrical Correlation

The two bottom hadrons in a $b\bar{b}$ event tend to be produced back-to-back, and their decay products are therefore likely to hit geometrically opposite parts of the detector. This introduces an efficiency correlation if the efficiency of the detector is not spatially uniform. This type of correlation can be estimated by measuring the hemisphere tagging probability in the data as a function of the thrust axis direction as

$$C_b = \frac{4\langle f^+(\theta, \phi)f^-(\theta, \phi) \rangle}{\langle f^+(\theta, \phi) + f^-(\theta, \phi) \rangle^2}, \quad (13)$$

where f^+ (f^-) is the fraction of hemispheres in the $+z$ ($-z$) direction that are tagged, and the averages are taken over the full solid angle acceptance. The actual estimation was carried out in small bins of $|\cos\theta|$ and ϕ . The effect of statistical fluctuations in the measurement of f was assessed by a Monte Carlo technique. The size of the correlation effect, $C_b - 1$, was measured to be $(+0.44 \pm 0.13)\%$, $(+0.57 \pm 0.13)\%$ and $(+0.44 \pm 0.06)\%$ in the 1992, 1993 and 1994 data, respectively, where the errors are due to the data statistics. The effect of the light-flavour background on these estimates was checked using the Monte Carlo and found to be negligible.

An interdependence might be expected between the geometrical correlation and the primary vertex correlation because the LEP beam spot size, and hence the primary vertex resolution, differs significantly between the vertical and the horizontal directions. This ϕ -asymmetry causes a small geometrical correlation which has already been included in the estimate of the primary vertex correlation. The size of this effect was evaluated in the Monte Carlo by comparing the geometrical correlations obtained using the measured and the true primary vertices. The difference was found to be negligibly small ($\sim 0.01\%$).

An interdependence might arise also between the geometrical correlation and the kinematical correlation, since, in the presence of final state QCD radiation, the two b hadrons in the event may no longer be produced approximately back-to-back and can be directed into regions of the detector with different b tagging efficiency. This was studied in Monte Carlo events by estimating the geometrical

	Tag	Lepton	Vertex	Mixed	Combined
Primary vertex		0.00%	-0.95%	0.00%	-0.47%
Kinematical		-0.49%	+0.05%	-0.41%	-0.03%
Geometrical:	1992	+1.56%	+0.38%	+0.34%	+0.44%
	1993	+1.62%	+0.65%	+0.33%	+0.57%
	1994	+0.95%	+0.39%	+0.43%	+0.44%
Total:	1992	+1.07%	-0.52%	-0.07%	-0.06%
	1993	+1.13%	-0.25%	-0.08%	+0.07%
	1994	+0.46%	-0.51%	-0.02%	-0.06%

Table 1: Hemisphere efficiency correlation $C_b - 1$ for each combination of tags. The ‘lepton’ and ‘vertex’ columns show the correlation calculated using the corresponding tags only. The ‘mixed’ column shows the correlation between the efficiencies of lepton and vertex tags in opposite hemispheres. The ‘combined’ column corresponds to the overall tag requiring either a lepton or a vertex in a hemisphere.

correlation using the true B hadron direction in place of the thrust axis direction, taking into account also the momentum dependence of the b tagging efficiency. The resulting change in the geometrical correlation estimate, 0.08%, is included in the systematic error when the total correlation is calculated.

6.4 Total Correlation

A summary of the primary vertex, kinematical and geometrical correlation estimates discussed above is given in Table 1. The correlations are given for the combined tag, requiring a lepton or a vertex in a given hemisphere, and also for the three separate possible combinations of lepton and vertex tags. The total correlation is obtained by summing the three separate components of the efficiency correlation. For the combined tag, the individual correlation components are small in magnitude ($<0.6\%$), and positive and negative contributions approximately cancel to leave a total correlation of size less than 0.1%.

It is important to ensure that correlations of different origin are independent of each other, so that the estimated effects correctly add up to the total correlation. Possible interdependences between the primary vertex, kinematical and geometrical correlations were discussed in the previous subsections. Significant interdependences were found only between the primary vertex and kinematic correlations, through the number of fragmentation tracks, and between the kinematic and geometrical correlations, and were included in the systematic error as described above.

It is also important to ensure that no significant correlation has been left out of the evaluation. To test this, the efficiency correlation estimated using the same methods as described above was compared with the true correlation in a large ($\sim 10^7$ events) sample of simulated $b\bar{b}$ events. The sample was generated using the same JETSET event generator but was processed by a fast simulation of the OPAL detector. Only the tracking detectors were simulated; thus only the vertex tagging was used in this test. Since we estimate the primary vertex correlation by measuring the difference between the total correlations obtained with measured and true primary vertices, the sum of the other components must be compared with the total correlation obtained using the true primary vertex. The result is shown in Figure 6. The true correlation agrees with the sum of the estimated components within the statistical errors for all L/σ_L cut values above 2. The difference at the final cut of $L/\sigma_L > 8$ is $(-0.18 \pm 0.15)\%$, where the error is statistical. A systematic error of $\pm 0.18\%$ was included in the estimate of the total correlation.

The systematic errors on the estimated correlation for the combined tag are summarised in Table 2. In total, the efficiency correlation between the two hemispheres of a $b\bar{b}$ event is estimated to be

Primary vertex:	MC statistics		$\pm 0.13\%$
	Detector resolution		$\pm 0.14\%$
	LEP beam spot size		$\pm 0.06\%$
	b fragmentation		$\pm 0.03\%$
	b lifetime		$\pm 0.01\%$
	b decay multiplicity		$\pm 0.04\%$
Kinematical:	Same-hemisphere events		$\pm 0.16\%$
	p_B - $p_{\bar{B}}$ correlation		$\pm 0.21\%$
	N_{frag} effect		$\pm 0.19\%$
Geometrical:	Data statistics	1992	$\pm 0.13\%$
		1993	$\pm 0.13\%$
		1994	$\pm 0.06\%$
Interdependence			$\pm 0.12\%$
Method			$\pm 0.18\%$
Total		1992	$\pm 0.46\%$
		1993	$\pm 0.46\%$
		1994	$\pm 0.45\%$

Table 2: Systematic errors on the hemisphere efficiency correlation $C_b - 1$.

$C_b - 1 = (-0.06 \pm 0.46)\%$, $+(0.07 \pm 0.46)\%$ and $(-0.06 \pm 0.45)\%$ for the 1992, 1993 and 1994 data, respectively. The errors are correlated between years except for those from the geometrical correlation, which come from the data statistics.

In the previous publication [2], the total correlation was estimated as $C_b - 1 = (+0.59 \pm 0.32)\%$, which differs from the estimates given here for the 1992 and 1993 data by more than the quoted uncertainty. There are two main reasons for this difference: firstly, the correlation through the primary vertex was hidden by the Monte Carlo statistical error, and was underestimated in the previous publication; secondly, the effect of fragmentation tracks in the kinematical correlation had not been found. These problems have been overcome in the new estimates. The uncertainties in the new estimates are dominated by the statistical errors in the comparisons between the real data and the Monte Carlo simulation, while in the old estimate, different Monte Carlo generators were compared with each other to estimate the systematic error. The possibility of interdependences between correlations of different origin and the completeness of the method itself have now been tested more carefully, resulting in small additional systematic errors. The new estimate of the correlation presented above, as well as its systematic error, is therefore more reliable than the one quoted in [2].

As discussed in Section 2, the correlation factors C_c and C_{uds} for light flavour events are set to unity (see equation (6)). About 0.3% of double-tagged events arise from $Z^0 \rightarrow c\bar{c}$ decays, while the fraction of double-tagged events from $Z^0 \rightarrow u\bar{u}, d\bar{d}, s\bar{s}$ decays is less than 0.01%. Even a hemisphere efficiency correlation as large as 10% in $c\bar{c}$ events would change R_b by only 0.00006, while efficiency correlations in $u\bar{u}, d\bar{d},$ and $s\bar{s}$ events have a negligible effect.

7 Result

The numbers of tagged hemispheres and double-tagged events found in the sample of 1 517 282 selected hadronic events are listed in Table 3. The symbols N_i denote the numbers of hemispheres tagged by i ,

		1992	1993	1994
Number of events	N_{had}	343 731	403 108	770 443
Tagged hemispheres	N_{ℓ}	8 455.2	9 975.9	18 661.3
	$N_{\text{v}} - N_{\bar{\text{v}}}$	29 488	33 874	67 463
	$N_{\text{a}} - N_{\bar{\text{v}}}$	36 561.2	42 297.9	83 047.3
Double-tagged events	$N_{\ell\ell}$	186.6	246.9	454.4
	$N_{\text{vv}} - N_{\text{v}\bar{\text{v}}} + N_{\bar{\text{v}}\bar{\text{v}}}$	2 645	2 994	6 024
	$N_{\ell\text{v}} - N_{\ell\bar{\text{v}}}$	1 486.6	1 738.5	3 297.6
	$N_{\text{aa}} - N_{\text{a}\bar{\text{v}}} + N_{\bar{\text{v}}\bar{\text{v}}}$	4 018.2	4 608.5	9 056.5

Table 3: Numbers of tagged hemispheres and double-tagged events in each year of the data. Background in the lepton samples has been subtracted. The numbers of hemispheres tagged by leptons, N_{ℓ} , is slightly smaller than the sum of the numbers of hemispheres tagged by electrons and muons given in Section 5.1 because a small number of hemispheres that contain both electrons and muons were counted only once.

Tag	Year	ϵ^c (%)	ϵ^{uds} (%)
ℓ	1992	0.353 ± 0.006	0.0113 ± 0.0009
	1993	0.349 ± 0.006	0.0111 ± 0.0009
	1994	0.344 ± 0.006	0.0109 ± 0.0009
$\text{v} - \bar{\text{v}}$	1992	1.025 ± 0.011	0.0973 ± 0.0040
	1993	0.992 ± 0.011	0.0973 ± 0.0040
	1994	1.025 ± 0.011	0.0973 ± 0.0040
$\text{a} - \bar{\text{v}}$	1992	1.374 ± 0.012	0.1083 ± 0.0041
	1993	1.337 ± 0.012	0.1082 ± 0.0041
	1994	1.364 ± 0.012	0.1080 ± 0.0041

Table 4: Percentage hemisphere tagging probabilities for light quark events estimated from the Monte Carlo for each year of the data. Errors are due to Monte Carlo statistics and are correlated between years.

where

$$i = \begin{cases} \ell & \text{for either electrons or muons,} \\ \text{v} & \text{for forward vertices,} \\ \bar{\text{v}} & \text{for backward vertices,} \\ \text{a} & \text{for either leptons or forward vertices.} \end{cases}$$

The symbols N_{ij} denote the numbers of double-tagged events with one hemisphere tagged by i and the other by j . The photon conversion and hadronic backgrounds to the identified lepton samples were subtracted from the totals before solving for R_{b} and ϵ^{b} because they were determined inclusively for the lepton-tagged samples. Incorrectly reconstructed vertices, on the other hand, are included in the light quark hemisphere tagging probabilities ϵ^c and ϵ^{uds} , since they are estimated from Monte Carlo separately for the different event flavours.

The hemisphere tagging probabilities for light quark events, estimated using the Monte Carlo events, are given in Table 4. The tagging probabilities vary slightly for each year of data because of small differences in the detector acceptance and performance. The Monte Carlo predicted no significant difference between the tagging probabilities for $u\bar{u}$, $d\bar{d}$ and $s\bar{s}$ events. The effect on R_{b} of treating $u\bar{u}$, $d\bar{d}$ and $s\bar{s}$ events together was estimated to be smaller than 10^{-6} . The predicted efficiencies for b quark events are not relevant for this analysis, since the b tagging efficiencies are determined directly

Tag	1992	1993	1994	Average	
ε^b	lepton	0.0460 ± 0.0035	0.0516 ± 0.0034	0.0511 ± 0.0024	0.0501 ± 0.0017
	lepton (mixed)	0.0530 ± 0.0014	0.0540 ± 0.0013	0.0513 ± 0.0009	0.0524 ± 0.0007
	vertex	0.1904 ± 0.0033	0.1871 ± 0.0031	0.1892 ± 0.0022	0.1889 ± 0.0016
	vertex (mixed)	0.1849 ± 0.0047	0.1831 ± 0.0044	0.1856 ± 0.0031	0.1848 ± 0.0022
	overall	0.2326 ± 0.0032	0.2303 ± 0.0030	0.2306 ± 0.0021	0.2310 ± 0.0015
R_b	lepton	0.2520 ± 0.0188	0.2265 ± 0.0149	0.2236 ± 0.0105	0.2308 ± 0.0079
	vertex	0.2124 ± 0.0037	0.2118 ± 0.0035	0.2184 ± 0.0025	0.2152 ± 0.0018
	mixed	0.2187 ± 0.0054	0.2163 ± 0.0052	0.2227 ± 0.0037	0.2201 ± 0.0026
	overall	0.2151 ± 0.0030	0.2144 ± 0.0029	0.2202 ± 0.0020	0.2175 ± 0.0014

Table 5: Values of R_b and ε^b after correlation correction. The efficiencies marked ‘mixed’ were obtained from the mixed-tagged events. Only statistical errors are included.

from the data.

Table 5 summarises the values of R_b and the b hemisphere tagging efficiency, ε^b , obtained by solving Equations (1) and (5). The measurements labelled ‘lepton’ and ‘vertex’ are statistically independent measurements obtained using lepton tags (N_ℓ and $N_{\ell\bar{\ell}}$) or vertex tags ($N_v - N_{\bar{v}}$ and $N_{v\bar{v}} - N_{v\bar{v}} + N_{\bar{v}\bar{v}}$) alone. Events with one hemisphere tagged by a lepton and the other by a vertex, referred to as ‘mixed’ events, provide a third measurement of R_b . In this case, the combination of N_ℓ , $N_v - N_{\bar{v}}$ and $N_{\ell v} - N_{\ell\bar{v}}$ is used to determine the three unknowns R_b , ε_ℓ^b and $\varepsilon_v^b - \varepsilon_{\bar{v}}^b$. Finally, the overall result is given by the combination of $N_a - N_{\bar{v}}$ and $N_{aa} - N_{a\bar{v}} + N_{\bar{v}\bar{v}}$, and includes all the statistics of the above three combinations. The values of R_b obtained from the lepton, vertex and mixed tags for the different years of data taking agree with each other at a χ^2 value of 10.9 for 8 degrees of freedom.

The R_b and ε^b values in Table 5 have been corrected for the effects of the $e^+e^- \rightarrow \tau^+\tau^-$ background, for the flavour-bias introduced by the event selection, and for the effect of the hemisphere tagging efficiency correlation. For the combined lepton and vertex tag, for the full data sample, the result $R_b = 0.2175 \pm 0.0014$ is obtained, where the error is due to the data statistics only. The statistical errors on the Monte Carlo estimates of the tagging probabilities, the uncertainty on the $\tau^+\tau^-$ background and flavour bias corrections, and the error on the efficiency correlation C_b will be included in the systematic error estimate discussed in the next Section.

8 Systematic Errors

The result of the measurement depends on R_c as:

$$\frac{\Delta R_b}{R_b} = -0.084 \frac{\Delta R_c}{R_c},$$

where ΔR_c is the deviation of R_c from the value of 0.172 predicted by the Standard Model and used in this analysis. For illustration, a fractional variation of ΔR_c of $\pm 5\%$, corresponding to the present precision of measurements at LEP [21], would result in a variation of ∓ 0.0009 in R_b .

The systematic errors coming from sources other than R_c are listed below, and are summarised in Table 6. Most of the systematic errors come through the tagging efficiencies, ε^c and ε^{uds} , for charm and light quark events. The dependence of R_b on ε^c and ε^{uds} is given by

$$\frac{\Delta R_b}{R_b} = -0.089 \frac{\Delta \varepsilon^c}{\varepsilon^c} - 0.027 \frac{\Delta \varepsilon^{\text{uds}}}{\varepsilon^{\text{uds}}}.$$

The systematic errors on these efficiencies are also given in Table 6.

Source	$\Delta\varepsilon^c/\varepsilon^c$ (%)	$\Delta\varepsilon^{\text{uds}}/\varepsilon^{\text{uds}}$ (%)	ΔR_b
Electron ID efficiency	± 0.50	± 0.22	± 0.00011
Muon ID efficiency	± 0.40	± 0.13	± 0.00009
Tracking resolution	± 0.76	± 3.69	± 0.00036
c quark fragmentation	± 2.89	—	± 0.00056
c hadron production fractions	± 3.05	—	± 0.00058
c hadron lifetimes	± 0.71	—	± 0.00014
c semileptonic branching fraction	± 0.95	—	± 0.00019
c semileptonic decay modelling	± 1.26	—	± 0.00024
c charged decay multiplicity	± 2.09	—	± 0.00040
Branching fraction $B(D \rightarrow K^0)$	± 1.19	—	± 0.00023
Heavy quark production from gluons	± 0.55	± 7.69	± 0.00055
K^0 and hyperon production	—	± 1.88	± 0.00011
Monte Carlo statistics	± 0.92	± 3.82	± 0.00034
Subtotal $\Delta\varepsilon^c$ and $\Delta\varepsilon^{\text{uds}}$	± 5.35	± 9.54	± 0.00124
Electron ID background			± 0.00036
Muon ID background			± 0.00040
Efficiency correlation			± 0.00098
Event Selection			± 0.00033
Total			± 0.00170

Table 6: Systematic errors on the measured value of R_b and on the light quark efficiencies ε^c and ε^{uds} .

Electron identification: The systematic errors related to the electron identification were evaluated using the methods described in reference [15].

The electron detection efficiency in the Monte Carlo, which was used to predict the tagging efficiency for the light flavour events, was tuned to agree with the data by applying corrections to the identifying variables. Remaining differences in the distributions of the variables were studied using subsamples of tracks in different angular, momentum and transverse momentum ranges, and using identified muon candidates. The flavour dependence of the efficiency caused by the difference in the track environment was studied in the Monte Carlo and a $\pm 50\%$ relative uncertainty was assigned to the predicted variation with flavour. The overall uncertainty in the electron detection efficiency was found to be $\pm 4.0\%$, which results in a systematic error on R_b of ± 0.00011 .

The number of electron candidates rejected by the photon conversion finding algorithm, and the performance of the algorithm predicted by the Monte Carlo, were used to estimate the background from photon conversion electrons in the identified electron sample. The efficiency of rejecting photon conversions and the probability of the rejected tracks really being conversion products were estimated using the Monte Carlo to be $(78.1 \pm 5.6)\%$ and $(78.6 \pm 4.0)\%$, respectively. The uncertainty on the conversion background resulted in a systematic error on R_b of ± 0.00026 . The hadronic background in the identified electron sample was estimated from the data using the distributions of the identifying variables. The relative uncertainty in the estimate of this background was found to be $\pm 9.3\%$, which results in a systematic error of ± 0.00025 on R_b .

Muon identification: The systematic errors related to the muon identification were evaluated using the methods described in reference [16].

The muon detection efficiency was compared between the Monte Carlo and the data using various control samples, e.g., muon pair events from Z^0 decays and two-photon collisions, and

identified charged pions from K^0 decays. After applying small corrections to the Monte Carlo, the uncertainty in the muon detection efficiency was found to be $\pm 3.0\%$, which results in a systematic error on R_b of ± 0.00009 . No significant flavour dependence was observed in the muon identification.

The hadronic background in the identified muon sample was estimated using the fake probability per track estimated in the Monte Carlo. Studies using several background control samples showed that the estimate had a relative uncertainty of $\pm 9\%$. The resulting systematic error is ± 0.00040 .

Tracking resolution: The resolution of the tracking detector strongly affects the vertex tagging efficiency. The effect was evaluated using the Monte Carlo by varying the resolution scaling factor β between 1.0 and 1.4. Although the forward tagging efficiency, ε_v , and the backward tagging efficiency, $\varepsilon_{\bar{v}}$, changed significantly with β , the difference $\varepsilon_v - \varepsilon_{\bar{v}}$ remained relatively stable (see Figures 3 and 4). The systematic error on R_b was found to be ± 0.00036 .

Charm quark fragmentation: The charm tagging efficiency ε^c increases with the scaled energy, x_E , of the weakly-decaying charmed hadron. OPAL has measured $\langle x_E \rangle$ separately for primary D^0 and D^+ mesons [22]. Using the relative D^0 and D^+ production cross-sections measured also in [22], the average scaled energy for D^0 and D^+ is $\langle x_E \rangle_{D^0, D^+} = 0.486 \pm 0.013$. Another measurement using leptons from charmed hadron decays by ALEPH [23] has obtained a consistent result.

The fragmentation function of Peterson et al. [14] was used to describe the charm quark fragmentation. The systematic error was studied by effectively varying the parameter ϵ_c by giving a weight to each $c\bar{c}$ event so that the mean scaled energy for D^0 and D^+ mesons varied within $\langle x_E \rangle_{D^0, D^+} = 0.486 \pm 0.013$. The resulting systematic error on R_b was ± 0.00056 .

Charmed hadron production fractions: The mixture of weakly decaying charmed hadrons produced in $Z^0 \rightarrow c\bar{c}$ decays can affect the tagging probability for $c\bar{c}$ events because of the large differences in the charm hadron lifetimes. The vertex tagging efficiency for the D^+ meson is approximately twice that for the D^0 and D_s^+ mesons, while the efficiency for the Λ_c^+ is about 20% of that for the D^0 and D_s^+ . The fractions of D^0 , D^+ , D_s^+ and Λ_c^+ were varied according to the production cross-sections measured by OPAL [22]. The contribution from Λ_c^+ baryons was multiplied by 1.15 ± 0.05 to account for the other weakly-decaying charmed baryons. The errors were combined taking their correlation into account to give a systematic error on R_b of ± 0.00058 .

Charmed hadron lifetimes: The lifetimes of the weakly-decaying charmed hadrons were varied within the errors quoted by the Particle Data Group [18]. Their contributions to the error on R_b were added in quadrature to give a total error of ± 0.00014 .

Charm semileptonic branching fraction: For semileptonic decays of charmed hadrons, an average branching fraction $B(c \rightarrow \ell)$ of $(9.8 \pm 0.5)\%$ was used. This value was obtained by taking the average of the measurements at centre-of-mass energies between 9.5 and 39 GeV [24]. The resulting systematic error was ± 0.00019 .

Charm semileptonic decay modelling: The momentum spectra of the leptons in the rest frame of the decaying charmed hadrons were modified according to the refined free-quark model of Altarelli et al. [25]. The two parameters of the model, m_s and p_F , were chosen to be $0.001 \text{ GeV}/c^2$ and $0.467 \text{ GeV}/c$, respectively, as given by a fit to DELCO [26] and MARK III [27] data performed by the LEP electroweak heavy flavour working group. Two sets of alternative values of the parameters, $m_s = 0.001 \text{ GeV}/c^2$, $p_F = 0.353 \text{ GeV}/c$ and $m_s = 0.153 \text{ GeV}/c^2$, $p_F = 0.467 \text{ GeV}/c$, corresponding to the variation allowed by the fit, were used to estimate the systematic error of ± 0.00024 .

Charm charged decay multiplicity: The requirement that a secondary vertex contain at least four tracks makes the tagging efficiency for a charmed hadron depend strongly on the charged track multiplicity of its decay. The distributions of the number of charged particles produced in the decays of D^+ , D^0 and D_s^+ mesons (including the charged decay products of any K_S^0 mesons produced in the D meson decay) were adjusted to the central values measured by MARK III [28]. The average decay charged multiplicity for each D meson was varied within the ranges quoted by MARK III, by applying an appropriate weight to each Monte Carlo event. For the Λ_c^+ baryon, for which no measurements are available, a variation of ± 0.5 in the average decay multiplicity was allowed. The average multiplicities were varied separately for each charm hadron, and in such a way as to leave the inclusive branching ratios for decays into K^0 mesons and Λ^0 hyperons unaltered. The resulting variations in R_b were combined in quadrature to give a systematic error on R_b of ± 0.00040 .

Charm to K^0 branching fraction: The inclusive branching ratios $B(D^+ \rightarrow K^0, \bar{K}^0 + X)$, $B(D^0 \rightarrow K^0, \bar{K}^0 + X)$, $B(D_s^+ \rightarrow K^0, \bar{K}^0 + X)$ and $B(\Lambda_c^+ \rightarrow \Lambda^0 + X)$ were varied independently within the errors quoted by the Particle Data Group [18]. This was done by applying a weight to each Monte Carlo event in such a way as to leave the decay charged multiplicity distribution for each charm hadron unaltered. The resulting variations in R_b were combined in quadrature to give a systematic error on R_b of ± 0.00023 .

Heavy quark production from gluon splitting: The average number of $c\bar{c}$ quark pairs produced per multihadron event by the gluon splitting process $g \rightarrow c\bar{c}$ has been measured by OPAL to be $(2.38 \pm 0.48) \times 10^{-2}$ [29]. This is consistent both with perturbative QCD calculations [30] and with the prediction of the JETSET Monte Carlo. The $g \rightarrow c\bar{c}$ rate in the Monte Carlo was adjusted to the OPAL measured value, and the $g \rightarrow b\bar{b}$ rate, for which no published measurements are available, was adjusted to be 0.13 ± 0.04 of the $g \rightarrow c\bar{c}$ rate, based on theoretical expectations [30]. The $g \rightarrow c\bar{c}$ rate and the $g \rightarrow b\bar{b}/g \rightarrow c\bar{c}$ ratio were varied separately within the ranges quoted, resulting in systematic errors on R_b of ± 0.00038 and ± 0.00040 , respectively. A total systematic error of ± 0.00055 was obtained by combining these errors in quadrature.

Inclusive K^0 and hyperon production: The total production rates of K^0 , Λ^0 and other weakly-decaying hyperons in the Monte Carlo were adjusted to agree with the values measured by OPAL [31]. The systematic error due to uncertainties in the number of weakly-decaying strange particles produced in $Z^0 \rightarrow u\bar{u}, d\bar{d}, s\bar{s}$ decays was assessed by allowing the average number of K^0 , Λ^0 and other hyperons in uds events to vary by $\pm 3.4\%$, $\pm 6.5\%$ and $\pm 11.5\%$, respectively. This corresponds to the precision of the OPAL measurements, combined with an additional uncertainty to take into account a possible flavour dependence in strange particle production rates in Z^0 decays. The separate variations in R_b were combined in quadrature to give a systematic error on R_b of ± 0.00011 .

Efficiency correlation: The total correlation factor was estimated to be $C_b - 1 = (-0.06 \pm 0.46)\%$, $(+0.07 \pm 0.46)\%$ and $(-0.06 \pm 0.45)\%$ for the 1992, 1993 and 1994 data, respectively, as was discussed in detail in Section 6. The resulting systematic error on R_b is ± 0.00098 .

Event Selection: As discussed in Section 4, a correction of $(-0.25 \pm 0.15)\%$ was applied to the result to account for the effects of the $e^+e^- \rightarrow \tau^+\tau^-$ background and the flavour-bias introduced by the event selection. The systematic error on R_b is ± 0.00033 .

Monte Carlo statistics: The Monte Carlo statistical errors in the evaluation of the light flavour tagging efficiencies contribute to the systematic error by ± 0.00034 .

The total systematic error on the measured value of R_b , excluding the R_c dependence, is ± 0.00170 .

As a cross check, the transverse momentum cuts for electrons and muons and the decay length significance cuts were varied within ± 0.3 GeV/ c and between 2 and 15, respectively. The values of R_b obtained using different cuts, and the independent part of the statistical error relative to the value of R_b obtained using the central cut values, are shown in Figure 7. No significant systematic trend in the measured value of R_b is observed.

9 Summary and Conclusion

The fraction of $Z^0 \rightarrow b\bar{b}$ events in hadronic Z^0 decays, R_b , was measured using the data collected by OPAL from 1992 to 1994, giving a result of

$$R_b = 0.2175 \pm 0.0014 \pm 0.0017$$

where the first error is statistical and the second systematic. The systematic error does not include the effects of varying R_c from its Standard Model expectation. The result depends on R_c as follows:

$$\frac{\Delta R_b}{R_b} = -0.084 \frac{\Delta R_c}{R_c},$$

where ΔR_c is the deviation of R_c from the value 0.172 predicted by the Standard Model. The total error excluding the R_c dependence is $\pm 1.02\%$ of the measurement. The result supersedes our previous publication [2] and the value quoted therein. The measurement of R_b presented here is consistent with other published measurements of R_b from experiments at LEP [32] and SLC [33], and is of improved precision.

The measured value of R_b is compared with the Standard Model prediction, obtained using the ZFITTER [3] program, in Figure 8. The value of R_d predicted by the Standard Model is also shown for comparison. The result is consistent within one standard deviation with the Standard Model prediction for top masses less than 182 GeV/ c^2 . The average result, 180 ± 12 GeV/ c^2 , of the CDF and D0 direct top mass measurements [34] is shown for comparison.

Acknowledgements

We particularly wish to thank the SL Division for the efficient operation of the LEP accelerator and for their continuing close cooperation with our experimental group. In addition to the support staff at our own institutions we are pleased to acknowledge the

Department of Energy, USA,

National Science Foundation, USA,

Particle Physics and Astronomy Research Council, UK,

Natural Sciences and Engineering Research Council, Canada,

Israel Science Foundation, administered by the Israel Academy of Science and Humanities,

Minerva Gesellschaft,

Japanese Ministry of Education, Science and Culture (the Monbusho) and a grant under the Monbusho International Science Research Program,

German Israeli Bi-national Science Foundation (GIF),

Direction des Sciences de la Matière du Commissariat à l'Énergie Atomique, France,

Bundesministerium für Bildung, Wissenschaft, Forschung und Technologie, Germany,

National Research Council of Canada,

Hungarian Foundation for Scientific Research, OTKA T-016660, and OTKA F-015089.

References

- [1] See for example: P. Bamert et al., Phys. Rev. D54 (1996) 4275, and references therein.
- [2] OPAL Collab., R. Akers et al., Z. Phys. C65 (1995) 17.
- [3] D. Bardin et al., CERN-TH 6443/92, May 1992.
- [4] OPAL Collab., K. Ahmet et al., Nucl. Instrum. Methods A305 (1991) 275.
- [5] P.P. Allport et al., Nucl. Instrum. Methods A324 (1993) 34.
- [6] P.P. Allport et al., Nucl. Instrum. Methods A346 (1994) 476.
- [7] M. Hauschild et al., Nucl. Instrum. Methods A314 (1992) 74;
O. Biebel et al., Nucl. Instrum. Methods A323 (1992) 169.
- [8] OPAL Collab., G. Alexander et al., Z. Phys. C52 (1991) 175.
- [9] JADE Collab., W. Bartel et al., Z. Phys. C33 (1986) 23;
JADE Collab., S. Bethke et al., Phys. Lett. B213 (1988) 235.
- [10] OPAL Collab., M.Z. Akrawy et al., Z. Phys. C49 (1991) 375.
- [11] T. Sjöstrand, Comp. Phys. Comm. 82 (1994) 74.
- [12] J. Allison et al., Nucl. Instrum. Methods A317 (1992) 47.
- [13] OPAL Collab., G. Alexander et al., Z. Phys. C69 (1996) 543.
- [14] C. Peterson, D. Schlatter, I. Schmitt and P. Zerwas, Phys. Rev. D27 (1983) 105.
- [15] OPAL Collab., R. Akers et al., Z. Phys. C60 (1993) 199.
- [16] OPAL Collab., P.D. Acton et al., Z. Phys. C58 (1993) 523.
- [17] ALEPH Collab., D. Buskulic et al., Phys. Lett. B357 (1995) 699;
ALEPH Collab., D. Buskulic et al., Z. Phys. C62 (1994) 179;
DELPHI Collab., P. Abreu et al., Z. Phys. C66 (1995) 323;
OPAL Collab., G. Alexander et al., Phys. Lett. B364 (1995) 93.
- [18] Particle Data Group, M. Aguilar-Benitez et al., Phys. Rev. D54 (1996) 1.
- [19] OPAL Collab., R. Akers et al., Z. Phys. C61 (1994) 209.
- [20] DELPHI Collab., P. Abreu et al., Phys. Lett. B347 (1995) 447.
- [21] The LEP Collaborations, ALEPH, DELPHI, L3, OPAL and the LEP Electroweak Working Group, CERN PPE/95-172.
- [22] OPAL Collab., G. Alexander et al., Z. Phys. C72 (1996) 1.
- [23] ALEPH Collab., D. Buskulic et al., Z. Phys. C62 (1994) 179.

- [24] CELLO Collab., H.J. Behrend et al., *Z. Phys.* C19 (1983) 291;
MARKJ Collab., B. Adeva et al., *Phys. Rev. Lett.* 51 (1983) 443;
TASSO Collab., M. Althoff et al., *Phys. Lett.* B146 (1984) 443;
TASSO Collab., M. Althoff et al., *Z. Phys.* C22 (1984) 219;
TPC Collab., H. Aihara et al., *Z. Phys.* C27 (1985) 39;
DELCO Collab., T. Pal et al., *Phys. Rev.* D33 (1986) 2708;
JADE Collab., W. Bartel et al., *Z. Phys.* C33 (1987) 339;
MARK II Collab., R.A. Ong et al., *Phys. Rev. Lett.* 60 (1988) 2587;
ARGUS Collab., H. Albrecht et al., *Phys. Lett.* B278 (1992) 202.
- [25] G. Altarelli et al., *Nucl. Phys.* B208 (1982) 365.
- [26] DELCO Collab., W. Bacino et al., *Phys. Rev. Lett.* 43 (1979) 1073.
- [27] MARK III Collab., R.M. Baltrusaitis et al., *Phys. Rev. Lett.* 54 (1985) 1976.
- [28] MARK III Collab., D. Coffman et al., *Phys. Lett.* B263 (1991) 135.
- [29] OPAL Collab., R. Akers et al., *Z. Phys.* C67 (1995) 27;
OPAL Collab., R. Akers et al., *Phys. Lett.* B353 (1995) 595.
- [30] M.H. Seymour, *Nucl. Phys.* B436 (1995) 163.
- [31] OPAL Collab., R. Akers et al., *Z. Phys.* C67 (1995) 389;
OPAL Collab., G. Alexander et al., CERN-PPE/96-99;
OPAL Collab., G. Alexander et al., CERN-PPE/96-100.
- [32] ALEPH Collab., D. Buskulic et al., *Phys. Lett.* B313 (1993) 535;
DELPHI Collab., P. Abreu et al., *Z. Phys.* C70 (1996) 531.
- [33] SLD Collab., K. Abe et al., *Phys. Rev.* D53 (1996) 1023.
- [34] CDF Collab., F. Abe et al., *Phys. Rev. Lett.* 74 (1995) 2626;
D0 Collab., S. Abachi et al., *Phys. Rev. Lett.* 74 (1995) 2632.

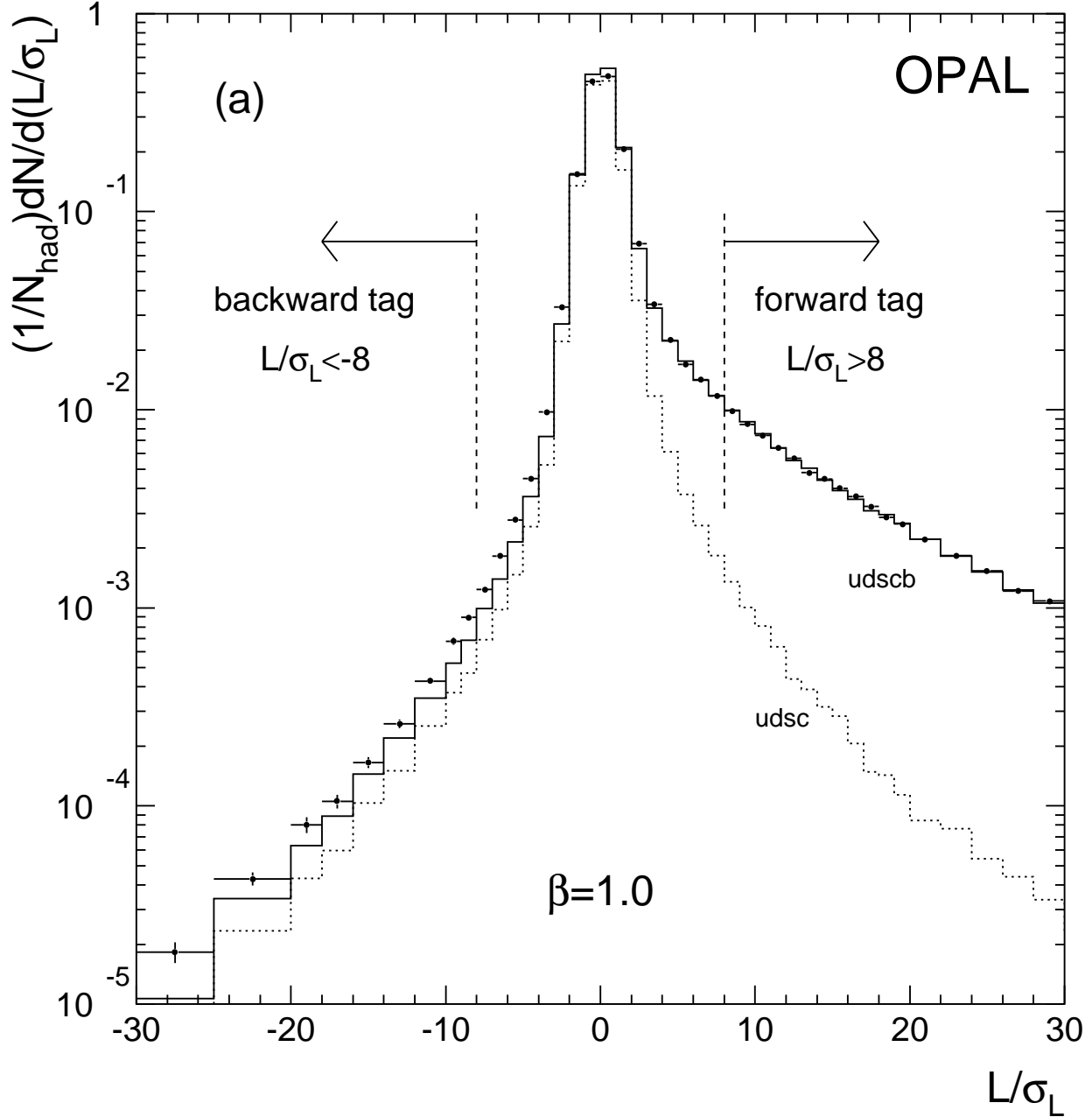
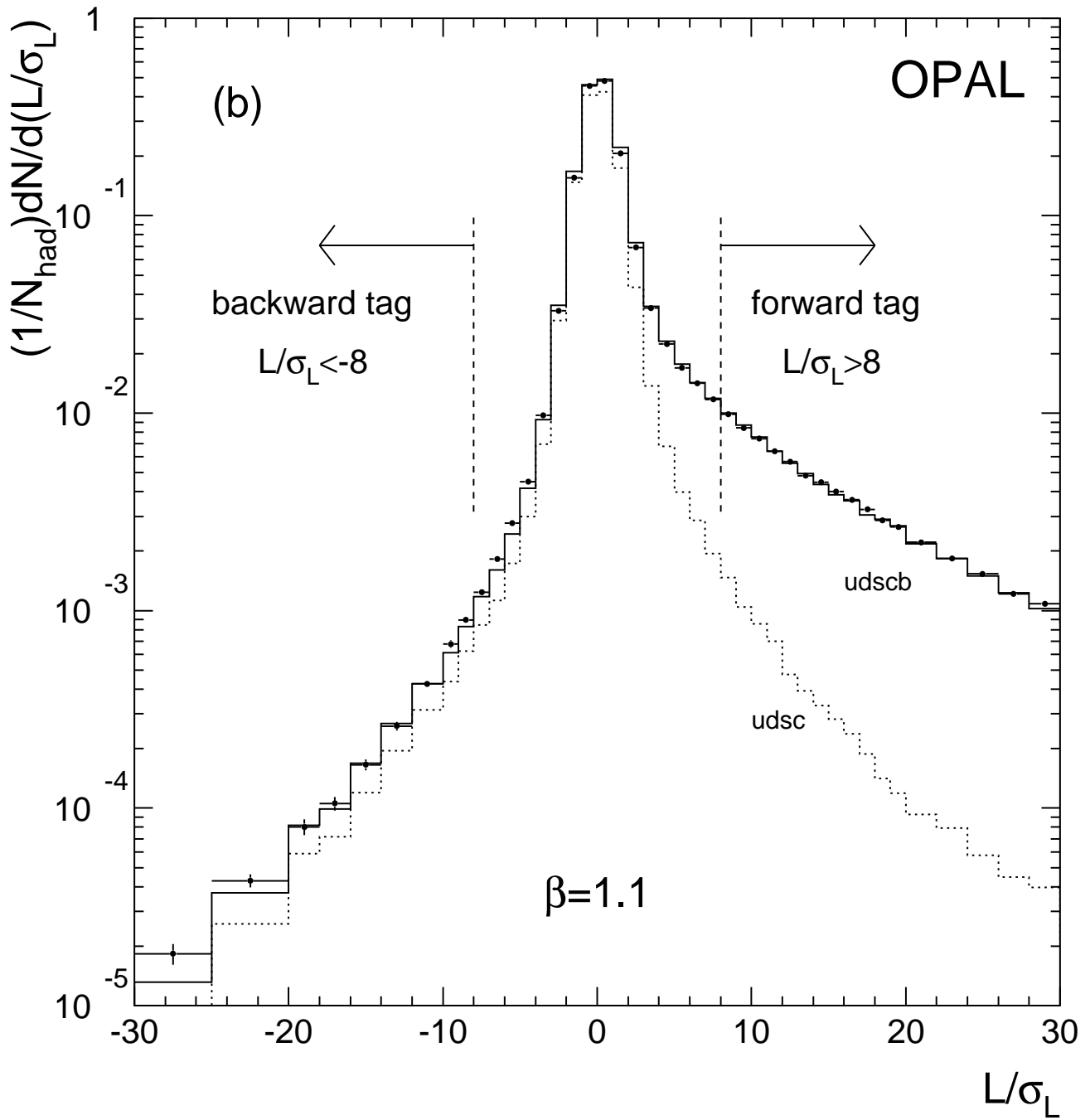


Figure 1: Comparison of L/σ_L distributions from the 1994 data (points with error bars) and from Monte Carlo (full histograms), normalised by the numbers of events. As discussed in the text, the most important region of the plot for this analysis is for backward decay length significances around the backward tag cut. Dotted histograms indicate contributions from light flavour events. In (b), the resolution in the Monte Carlo events has been degraded as described in the text with a scaling factor $\beta = 1.1$; no such scaling has been applied in (a).



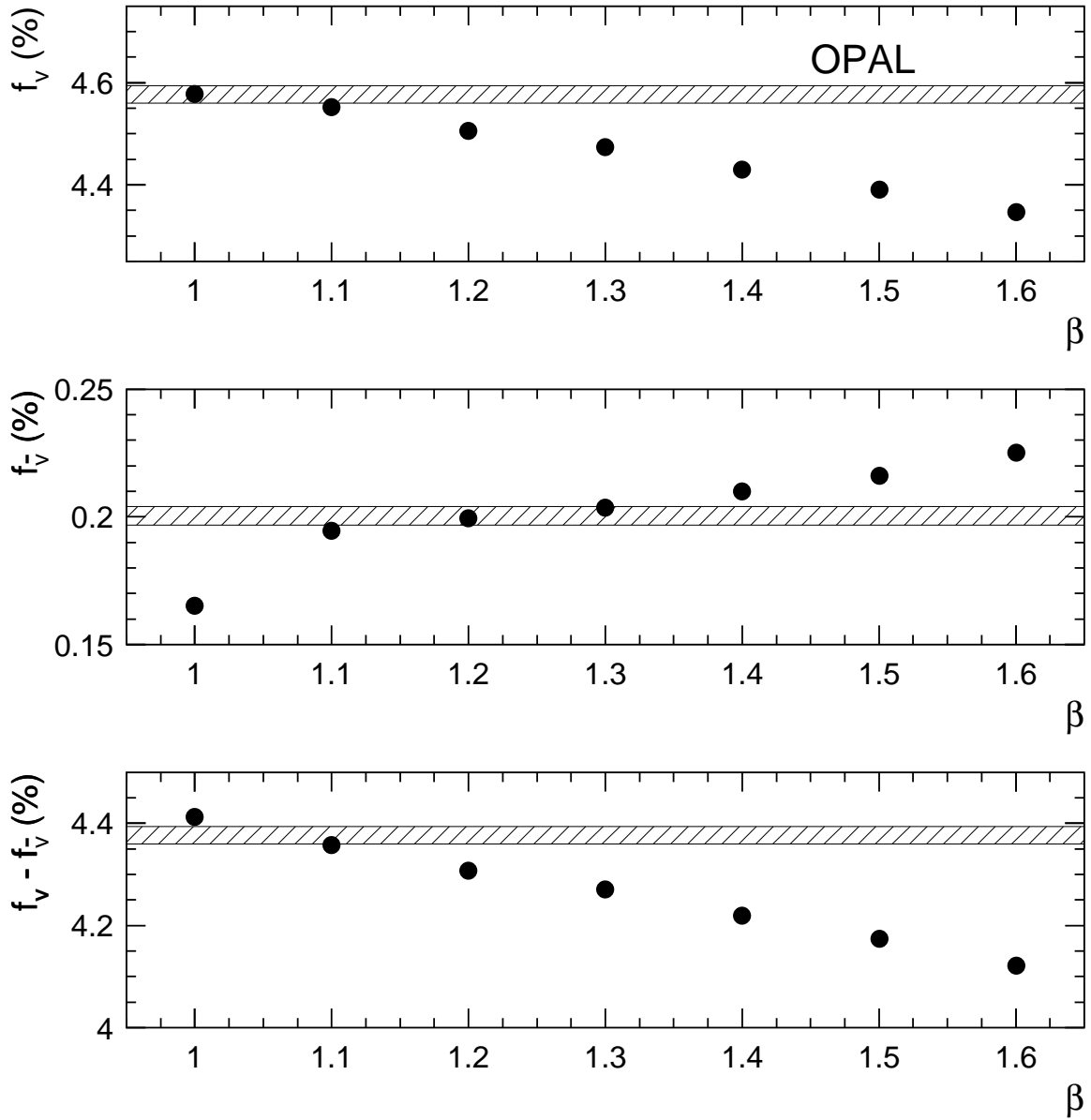


Figure 2: Forward and backward hemisphere tagging fractions, f_v and $f_{\bar{v}}$, from Monte Carlo simulation, and their difference, as a function of the resolution scaling factor β . The horizontal shaded regions indicate the tagging fractions measured in the 1994 data with their statistical errors.

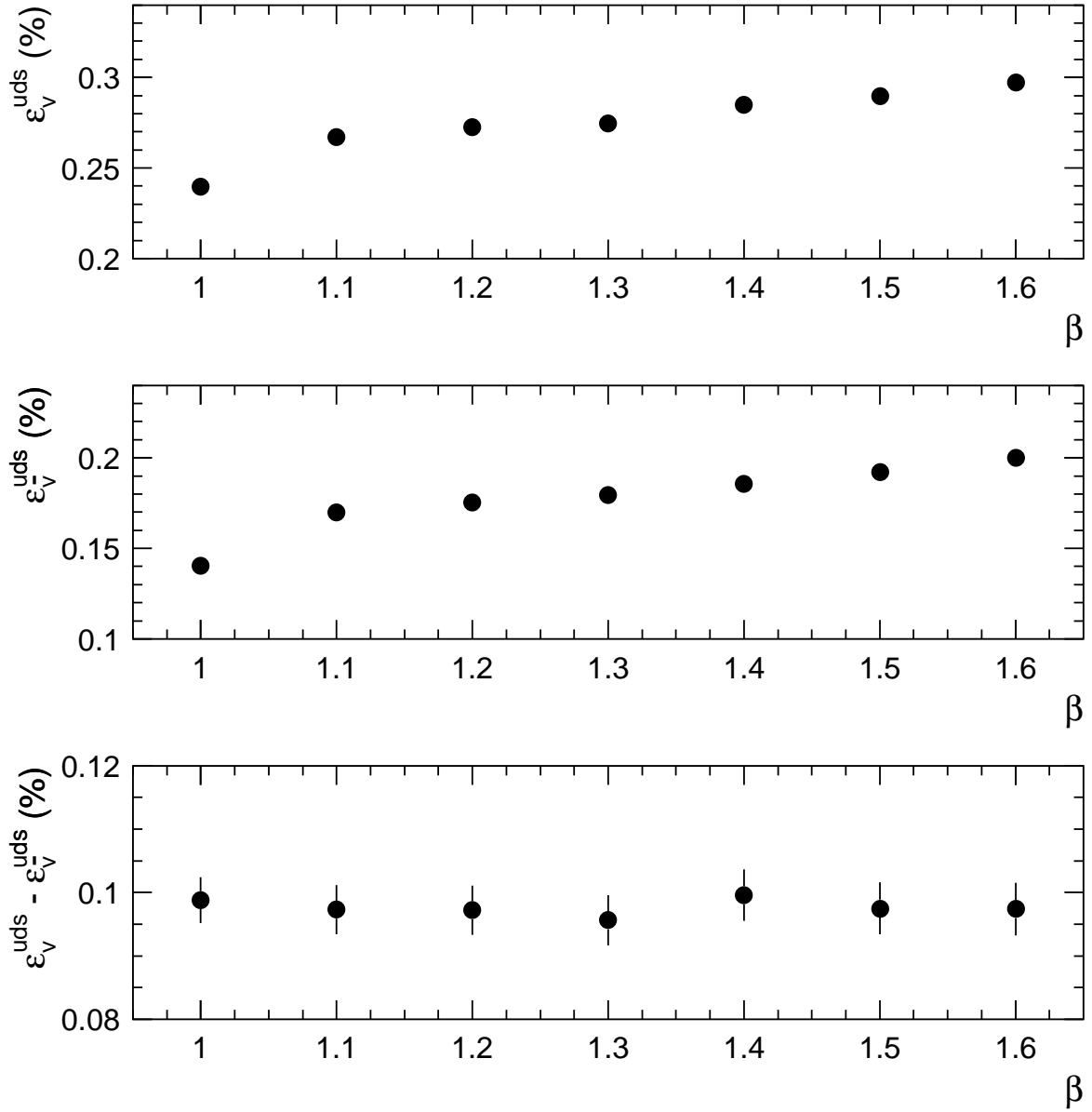


Figure 3: Forward and backward tagging efficiencies, ϵ_v^{uds} and $\epsilon_{\bar{v}}^{uds}$, from Monte Carlo simulated $Z^0 \rightarrow u\bar{u}, d\bar{d}, s\bar{s}$ events, and their difference, as a function of the resolution scaling factor β .

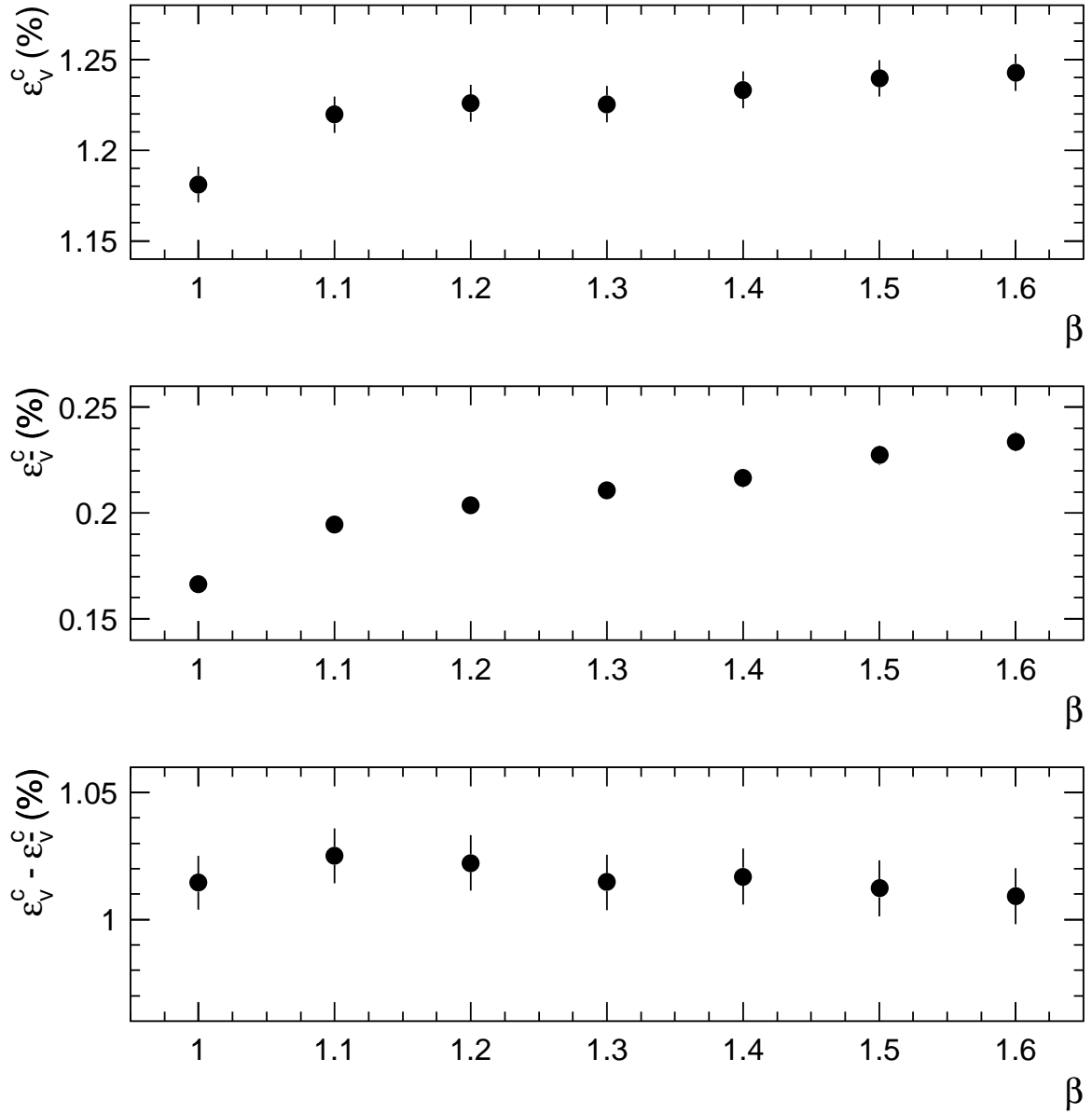


Figure 4: Forward and backward tagging efficiencies, ε_V^c and $\hat{\varepsilon}_V^c$, from Monte Carlo simulated $Z^0 \rightarrow c\bar{c}$ events, and their difference, as a function of the resolution scaling factor β .

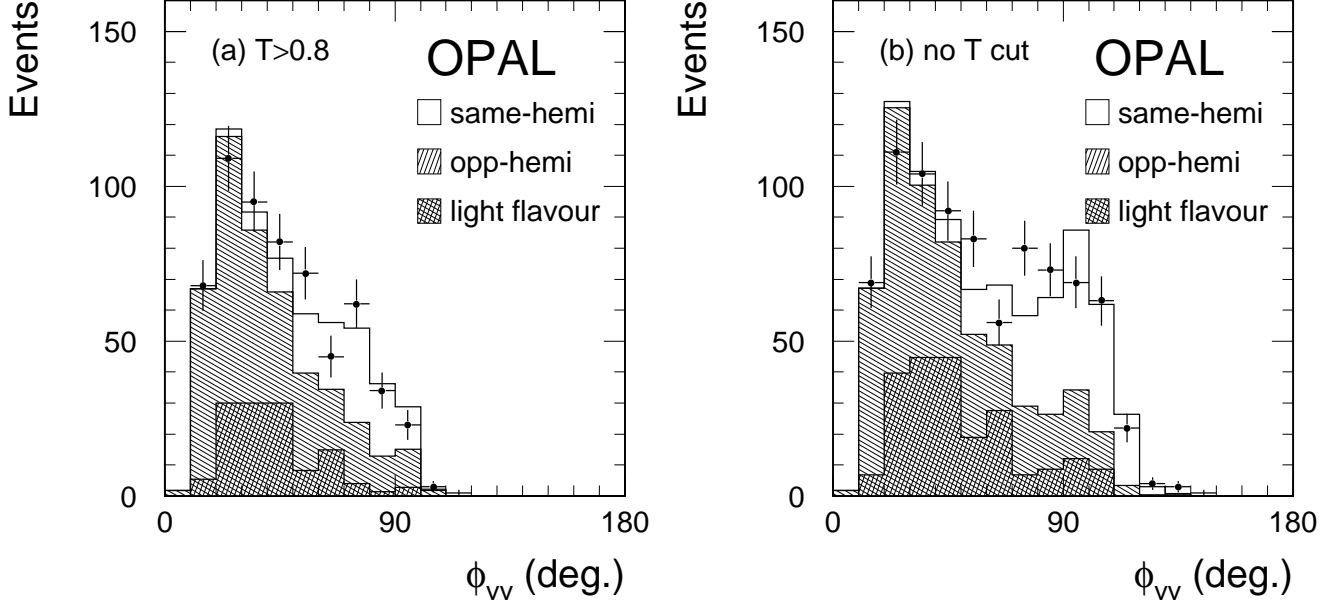


Figure 5: Fits of ϕ_{VV} distribution (a) with and (b) without the thrust value cut $T > 0.8$. Points with error bars are data and the histograms are Monte Carlo fitted to the data.

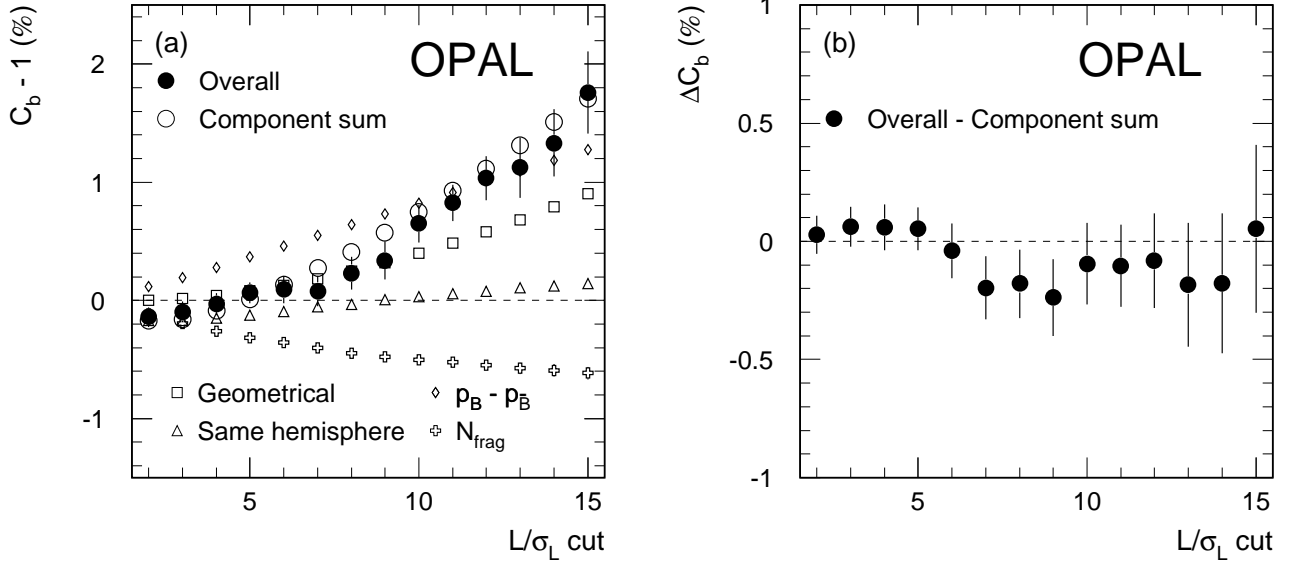


Figure 6: (a) Comparison between the true overall correlation (solid circles) and the sum of the estimated correlation components (open circles) in a large sample of $b\bar{b}$ Monte Carlo events, as a function of the L/σ_L cut. The individual components of the estimated correlation due to the geometrical correlation, same hemisphere $b\bar{b}$ events, the $p_B - p_{\bar{B}}$ correlation and the correlation from the N_{frag} effect are shown separately. The difference between the true and total estimated correlations is shown in (b).

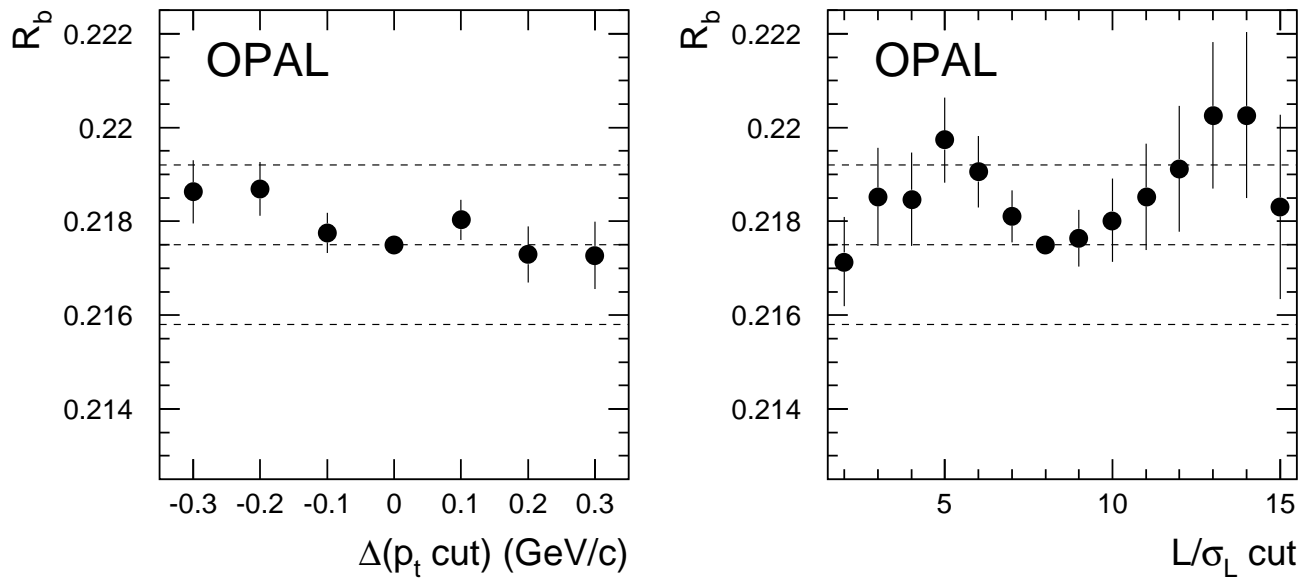


Figure 7: Values of R_b obtained using different cuts on the lepton transverse momentum p_t and the decay length significance L/σ_L . The results have been corrected for hemisphere tagging efficiency correlation. Dashed lines indicate the central value and its systematic error. Error bars are the statistical errors on the differences from the central result.

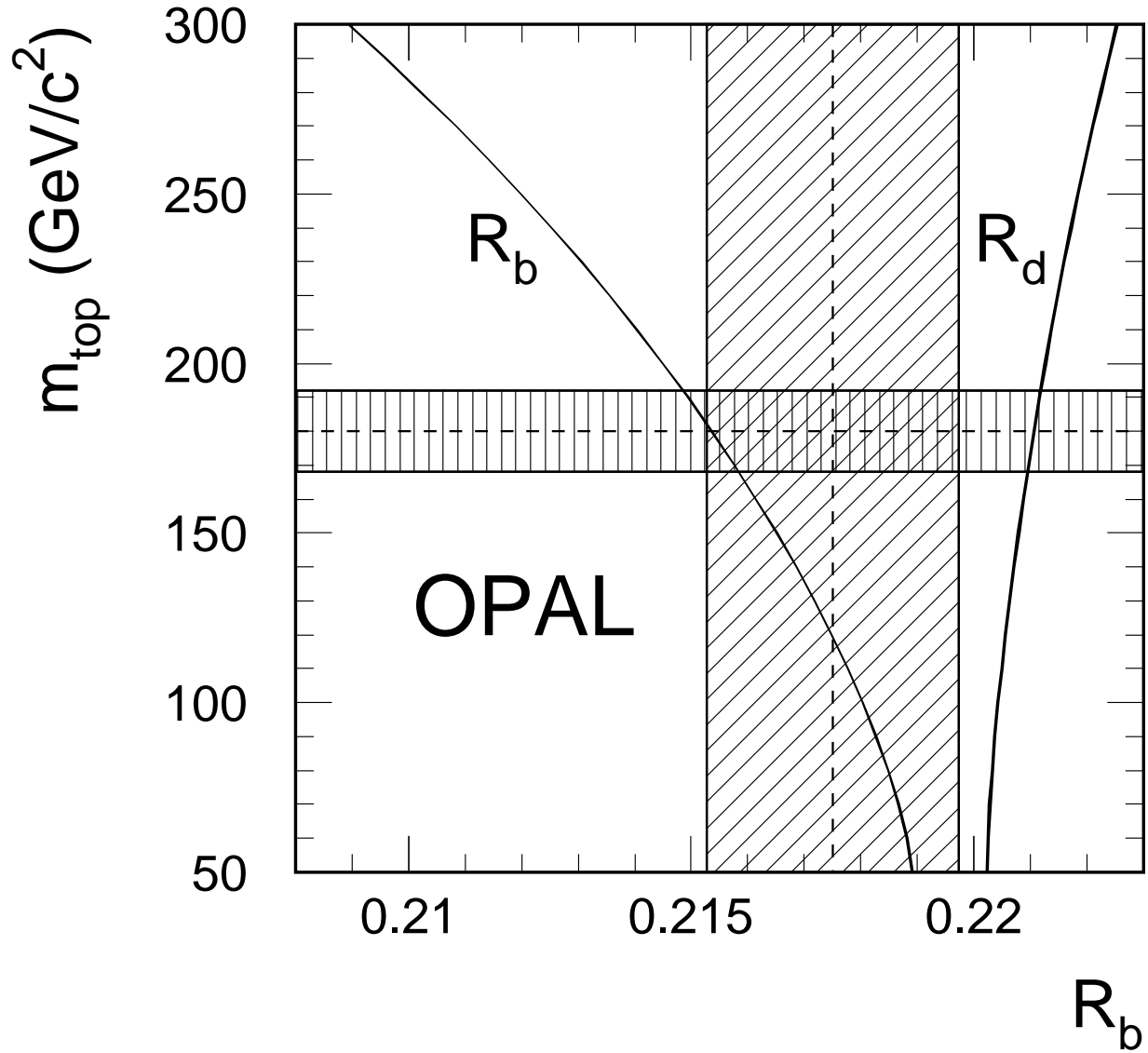


Figure 8: Comparison between the measured value of R_b , the Standard Model prediction obtained using the ZFITTER program, and the directly measured top mass from CDF and D0. The diagonally hatched area shows the plus-or-minus one standard deviation range of this measurement, and the vertically hatched region shows the CDF and D0 top mass measurement. Curves indicate the predicted values of R_b (left) and R_d (right) as functions of the top quark mass m_{top} . The widths of the curves represent the uncertainty due to Higgs boson masses in the range 60–1000 GeV/c^2 .